Proteomic responses under differing pH and pCO_2 levels in the diatom *Thalassiosira pseudonana* are consistent with a hybrid carbon concentrating mechanism

Anthony R. Himes and Adam B. Kustka

Department of Earth and Environmental Sciences, Rutgers University—Newark, 101 Warren Street, Newark, NJ 07102, USA.

Email addresses: anthony.himes@rutgers.edu, adam.kustka@rutgers.edu

Submission date: 11 June 2025

Number of tables: three

Number of figures: four

Word count: 6543

Supplemental data: One document, six tables

Running title: Proteomic analysis of the CCM of *T. pseudonana*

Highlight

Experimental manipulation of carbonate chemistry allowed for the separation of the carbon concentrating mechanism in *T. pseudonana* from other processes that rely on the same proteins, revealing a hybrid CCM.

Abstract

The effects of ongoing anthropogenic climate change are not well known in marine diatoms, a key group of primary producers. In particular, detailed characterizations of their carbon concentrating mechanisms (CCM) are lacking, which limits the understanding of how changing ocean carbonate chemistry will impact global primary production. While the model diatom *Thalassiosira pseudonana* has been widely studied, contrasting results have prevented the clear elucidation of its CCM. A quantitative proteomic analysis was therefore performed across three experimental treatments (low pCO_2/high pH, high pCO_2/low pH, low pCO_2/low pH) to discern the specific roles of proteins that can be involved in CCMs as well as other cellular processes (e.g. pH and redox regulation). This analysis revealed a hybrid CCM consisting of both biophysical and biochemical steps that facilitate increased CO_2 diffusion into the cell, the formation and transport of an organic carbon intermediate into the chloroplast, the subsequent decarboxylation of this intermediate, and the facilitated diffusion of inorganic carbon from the stroma into the pyrenoid-penetrating thylakoid. No evidence supporting alternative roles for the identified CCM proteins was found. As several aspects of this CCM require further investigation, common challenges inherent to CCM research are discussed and strategies to overcome them are suggested.

Keywords: acid-base regulation, alternative oxidase, CCM, carbon uptake, carbonate chemistry, carbonic anhydrase, malate dehydrogenase, malate/oxaloacetate shuttle, phosphoenolpyruvate carboxylase, proteome

Abbreviations: AOX, mitochondrial alternative oxidase; CA, carbonic anhydrase; CCM, carbon concentrating mechanism; CET, cyclic electron transport; ETC, electron transport chain; FDR, false discovery rate; HCLpH, high pCO_2/low pH; LCHpH, low pCO_2/high pH; LCLpH, low pCO_2/low pH; MDH, malate dehydrogenase; ME, malic enzyme; NDH, NADH-like complex; OAA, oxaloacetate; OMT, 2-oxoglutarate/malate translocator; PEP, phosphoenolpyruvate; PEPC, phosphoenolpyruvate carboxylase; PEPCK, phosphoenolpyruvate carboxykinase; PGR5, proton gradient regulation 5 protein; PGRL1, PGR5-like photosynthetic phenotype 1 protein; PTOX, plastidial terminal oxidase; PYC, pyruvate carboxylase; SDR, short-chain dehydrogenase/reductase family; SLC4, solute carrier family 4

Introduction

In the face of ongoing anthropogenic climate change, the need to further our understanding of how various taxonomic groups will be impacted is of ever-increasing importance. Marine phytoplankton are one key group, as they account for about half of all global primary production (Behrenfeld *et al.*, 2001; Westberry *et al.*, 2023). In particular, diatoms account for the largest proportion of marine planktonic primary production, with estimates ranging from 20 to 50% (Neslon *et al.*, 1995; Field *et al.*, 1998; Armbrust, 2009; Rousseaux and Gregg, 2014; Tréguer *et al.*, 2018). As anthropogenic carbon dioxide (CO_2) emissions continue to drive ocean acidification, the concomitant increase in oceanic partial

pressure of CO_2 (pCO_2) and decrease in pH will directly affect dissolved inorganic carbon (DIC) speciation, and therefore, have direct effects on all carbon fixing organisms (IPCC, 2023). However, the nature of these impacts are still unclear within diatoms as their mechanisms for DIC uptake and its subsequent transport through the cell to ribulose-1,5-bisphosphate carboxylase/oxygenase (RuBisCO), known collectively as carbon concentrating mechanisms (CCM), are not well understood (Granum *et al.*, 2005; Trimborn *et al.*, 2008; Reinfelder, 2011; Kustka *et al.*, 2014; Zhang *et al.*, 2014; Clement *et al.*, 2016; Wu *et al.*, 2021; Nam *et al.*, 2024; Shimakawa *et al.*, 2024).

There are two classes of CCMs broadly termed biophysical and biochemical based on whether a given mechanism relies solely on bicarbonate (HCO_3^-) pumping and CO_2 diffusion or includes the formation, transport, and decarboxylation of an acid-stable four carbon intermediate, respectively (see review by Reinfelder, 2011). Both concentrate CO_2 near RuBisCO, which in diatoms is localized to the pyrenoid to minimize photorespiratory losses (Edwards *et al.*, 2004; Mackinder *et al.*, 2016; Nam *et al.*, 2024; Shimakawa *et al.*, 2024). Biophysical CCMs in marine phytoplankton depend on the active transport of extracellular HCO_3^- through multiple subcellular compartments alongside various forms of carbonic anhydrase (CA) that help to prevent the diffusive loss of CO_2 (Tachibana *et al.*, 2011; Samukawa *et al.*, 2014; Tanaka *et al.*, 2014; Hennon *et al.*, 2015; Nawaly *et al.*, 2023b; Shimakawa *et al.*, 2023).

For biochemical CCMs, much understanding stems from vascular land plants, where C_4 plants are known to store inorganic carbon as four-carbon compounds before transport near to RuBisCO, and subsequent decarboxylation to release CO_2. One commonly observed C_4 plant CCM begins with phosphoenolpyruvate carboxylase (PEPC) converting cytosolic phosphoenolpyruvate (PEP) and CA-derived HCO_3^- into oxaloacetate (OAA). This OAA is then

reduced to malate by malate dehydrogenase (MDH) before transport into the chloroplast where $NADP^+$-dependent malic enzyme (ME) decarboxylates malate to pyruvate, NADPH + H^+, and CO_2. As RuBisCO is found within the chloroplast stroma of C_4 plants, the decarboxylation of malate concludes this form of CCM. Evidence from several studies also supports the existence of similar biochemical CCMs within some diatoms (Reinfelder *et al.*, 2004; Kustka *et al.*, 2014; Wu *et al.*, 2021; Yu *et al.*, 2022; Zhen *et al.*, 2025); however, in all cases, key differences have been observed between C_4 plant and diatom CCMs. One major difference recently noted in two model diatom species, *Thalassiosira pseudonana* and *Phaeodactylum tricornutum*, is the presence of a specialized protein coat surrounding the pyrenoid that may act as a diffusion barrier to CO_2, thereby requiring further CA-mediated steps to ultimately concentrate CO_2 near RuBisCO (Nawaly *et al.*, 2023b; Nam *et al.*, 2024; Shimakawa *et al.*, 2024).

Multiple studies have attempted to characterize the CCM of *T. pseudonana*, but have yielded inconsistent results with contrasting interpretations. (Reinfelder *et al.*, 2004; Roberts *et al.*, 2007; Granum *et al.*, 2009; Trimborn *et al.*, 2009; Kustka *et al.*, 2014; Tanaka *et al.*, 2014; Clement *et al.*, 2016; Hopkinson *et al.*, 2016). First, seemingly contradictory results on pCO_2-dependent changes in HCO_3^- uptake have been reported for *T. pseudonana* (Trimborn *et al.*, 2009; Clement *et al.*, 2016), although there were large differences between the "high" pCO_2 levels used in these studies. Second, relative transcript abundances for the two known PEPC genes (PEPC1 and PEPC2) have shown inconsistent sensitivities to steady-state pCO_2 conditions (Granum *et al.*, 2005; Roberts *et al.*, 2007; Tanaka *et al.*, 2014) compared to abrupt shifts from higher to lower pCO_2 levels (Granum *et al.*, 2009; Kustka *et al.*, 2014) leading to debate over the classification of the CCM of *T. pseudonana* as biophysical or biochemical. Third, while PEPC1 and PEPC2 protein abundances did not increase in line with their respective transcript levels

immediately following a shift from high to low pCO_2 (Granum *et al.*, 2009), they did increase in response to steady-state low pCO_2 conditions (Kustka *et al.*, 2014), which highlights that gene expression levels are not always representative of cellular physiology. Lastly, in vitro PEPC to RuBisCO activity ratios have been used to argue in favor of a biophysical CCM (Trimborn *et al.*, 2009; Clement *et al.*, 2016), although it remains unclear how representative these methodologies are of true in vivo PEPC activity in *T. pseudonana*.

One difficulty of elucidating a CCM is the accurate localization of its protein components. For example, early predicted localizations of PEPC2 placed it within the mitochondrial matrix of diatoms (Kroth *et al.*, 2008). Recent findings in other eukaryotic phototrophs, however, place it on the surface of mitochondria (O'Leary *et al.*, 2011; Park *et al.*, 2012; O'Leary and Plaxton, 2020), which is the same localization supported by current predictive tools for *T. pseudonana* (Ødum *et al.*, 2024). Accurate protein localizations are but one of the prerequisites to adequately understand protein function.

Several metabolic pathways are known that, if upregulated in response to changing pCO_2 and/or pH conditions, could be misinterpreted as evidence of a C_4 CCM. For example, upregulation of PEPC under low pCO_2/high pH conditions might be indicative of the intracellular pH homeostasis pathways described in Sakano (1998) where PEPC activity serves to acidify the cell. This acidification effect is then spread across subcellular compartments by the malate/OAA shuttle, which is the term given to the reduction of OAA to malate by MDH, the transport of malate across intracellular membranes, and its subsequent oxidation back to OAA by MDH (reviewed in Selinski and Scheibe, 2018). The malate/OAA shuttle is also known to be utilized to maintain cellular redox poise, facilitate cyclic electron transport, and dissipate excess light energy (Shikanai, 2007; Yoshida *et al.*, 2007; van Dongen *et al.*, 2011; Yu *et al.*, 2014;

Nawrocki *et al.*, 2015; Dietz *et al.*, 2016; Murik *et al.*, 2018; Selinski and Scheibe, 2018; Chadee *et al.*, 2021; Zhou *et al.*, 2021; Hippmann *et al.*, 2022; Degen *et al.*, 2024). However, none of these alternative mechanisms have been evaluated simultaneously with the CCM of *T. pseudonana*.

Given the debate surrounding the identity of the CCM in *T. pseudonana*, this study employed a quantitative proteomic approach across three experimental conditions to assess each step constituting the CCM of this species. The three conditions evaluated were 1) low pCO_2/high pH, 2) high pCO_2/low pH, and 3) low pCO_2/low pH. While *T. pseudonana* is unlikely to experience the third condition in a natural setting, as it was achieved by decreasing the total DIC pool, the inclusion of this treatment will help to disentangle any potential biochemical CCM from the aforementioned alternative mechanisms involving PEPC and the malate/OAA shuttle driven by changes in pH alone, irrespective of pCO_2. In this way, this study aims to clarify and deepen the understanding of both the CCM of *T. pseudonana* as well as various other cellular pathways that may be modulated in response to increases in pCO_2 and/or decreases in pH, thus providing insight into how diatoms as a whole will respond to ongoing ocean acidification.

Materials and methods

Stock culture conditions

Thalassiosira pseudonana (strain CCMP 1335) was maintained in a culture incubator (VWR, Radnor, PA, USA; Model No. 2015) set to 18°C with 24 h high-intensity light (250 μmol photons m^{-2} s^{-1}). Precision incubator thermometers (VWR) were maintained alongside

cultures and checked daily to ensure temperatures remained consistent. Stock cultures were grown in metal-replete Aquil* media following Sunda *et al.*, 2005, with the Fe concentration lowered to 600 nM and the treatment with Chelex-100 omitted. Synthetic seawater was combined with macronutrient, trace metal, and vitamin stock solutions (Sunda *et al.*, 2005) in clean sterile polycarbonate bottles (see supplemental *Cleaning and sterilization*) within a class 100 laminar flow hood (Mystaire, Creedmoor, NC, USA). Assembled media was vacuum filter sterilized using autoclaved 0.2 µm Supor PES membrane filter discs (Pall Corporation, Port Washington, NY, USA). *T. pseudonana* was then inoculated into sterile media contained within clean sterile 30 mL polycarbonate tubes. Semi-continuous batch cultures were maintained in this way for the duration of the study so that cells in logarithmic growth phase were readily available for experimentation. Growth of stock cultures was monitored daily by measuring relative chlorophyll a fluorescence using a Turner Designs 10-AU fluorometer (Turner Designs, San Jose, CA, USA). Growth rates were calculated from linear regressions of the natural logarithm of blank corrected relative chlorophyll a fluorescence over time in days.

Experimental culture media

T. pseudonana was exposed to three experimental treatments: a low pCO_2/high pH condition (pCO_2 = 202 µatm, pH = 8.48), a high pCO_2/low pH condition (pCO_2 = 1702 µatm, pH = 7.61), and a low pCO_2/low pH condition (pCO_2 = 202 µatm, pH = 7.61). Hereafter these treatments will be referred to as LCHpH, HCLpH, and LCLpH, respectively. The letters H and L denoted high or low, pCO_2 is shortened to the letter C, and pH is left unabbreviated. For each of the three treatments, metal-replete Aquil* was made following the same procedures outlined above, but with two key differences.

First, the concentration of $NaHCO_3$ in the LCLpH treatment was lowered from 2.38 mM to 0.283 mM so that at pH 7.61 the pCO_2 of this media would be equal to that of the LCHpH media. CO2SYS (Lewis and Wallace, 1998; see supplemental *CO2SYS constants*) was used to determine this lower DIC concentration while producing three treatments from two unique pH and pCO_2 levels that would serve to distinguish the impact of pH alone from the CCM of *T. pseudonana*. To prevent carbon limitation in LCLpH cultures while also limiting the potential for fluctuations in carbonate chemistry driven by high culture biomass (Shi *et al.*, 2009; Crawfurd *et al.*, 2011), all experimental cultures were sampled at relatively low biomass (~70,000 cells per mL^{-1}).

The second key difference in the experimental media was that the total concentration of each trace metal varied among treatments. This was done so that free metal ion concentrations would be equivalent across treatments despite their differences in carbonate chemistry (Sunda *et al.*, 2005). The total metal concentrations for each treatment were calculated using Visual MINTEQ ver. 4.0.

Once media was fully assembled and filter sterilized, a small aliquot was removed to measure pH using a freshly calibrated Oakton double-junction all-in-one pH/ATC electrode (Cole-Parmer 35811-72) connected to an Oakton pH 110 series pH meter (Cole-Parmer 35615-20). Dilute NaOH and HCl solutions, made in ultrapure water and 0.2 μm filter sterilized, were used to adjust culture media to the desired pH for each condition.

Experimental apparatus

Experiments were carried out in modified 500 mL polycarbonate bottles. In brief (see supplemental *Experimental apparatus continued* for full details), three modifications were made

to enable real-time pH monitoring and control: 1) an acid line was plumbed in through the neck of the bottle to deliver 0.006 M HCl, prepared in treatment-specific synthetic ocean water, to counteracted pH increases driven by photosynthetic activity. 2) An airline was run to the bottom of the bottle through which a mixture of ultra zero grade air and CO_2 (Airgas, Radnor, PA, USA) was bubbled to mix cultures during acid additions. High accuracy mixer rotameters (Matheson Tri-gas Inc., Montgomeryville, PA, USA) were used to ensure each experimental culture was bubbled with air matching its target pCO_2. 3) A Thermo Orion double junction pH electrode (Thermo Scientific 9156DJWP) was inserted through the cap of the bottle and was used to measure pH in real time throughout the course of each experimental trial. In each of three identical experimental systems, Alpha pH 200 series pH controllers (Eutech Instruments ECPHCTP0200) were used in conjunction with gas solenoid valves (ASCO U8256B045V) for air delivery and small peristaltic pumps (Masterflex C/L 77120-20) for acid delivery to maintain pH setpoints (similar to the setup used in Kustka *et al.*, 2014). These controllers were programmed to maintain pH within 0.02 pH units of the target level, which matched the reported precision for the pH probes. During testing, pH probe drift over the course of one week was negligible; therefore, pH probes were freshly calibrated at the start of each 4-day experimental trial. Culture pH was recorded twice daily for the duration of each trial.

A second air delivery system was used to refresh the headspace of each culture bottle with the appropriate pCO_2 gas mixture to minimize laboratory air intrusion as bottles could not be kept sealed while actively regulating pH. Solenoid valves were programmed to open every 15 min for a 2-min duration using outdoor plugs (Wyze Labs, Inc., Seattle, Washington, USA). During testing, this additional air turnover was found to markedly improve pH control.

Experimental trials

At the start of each experimental trial, 450 mL of sterile media was inoculated with mid-logarithmic growth phase *T. pseudonana*. Three cultures, one of each treatment group, were always run in parallel within the same incubator that was used to maintain stock cultures. Trials (n = 8) lasted for approximately 4 d and growth was monitored daily by measuring cell counts and biovolumes with a Multisizer 3 Coulter counter (Beckman Coulter Life Sciences, Indianapolis, IN, USA). Specific growth rates (μ) were then calculated from the linear regression of the natural logarithm of cell density (cell mL^{-1}) over time in days (Table S2). Experimental cultures were inoculated such that a minimum of 10 cell divisions occurred prior to sampling. Once cultures reached approximately 70,000 cells mL^{-1}, cells were collected via vacuum filtration onto 3 μm polycarbonate filter discs (MilliporeSigma). Cells were then transferred into microcentrifuge tubes and flash frozen in liquid nitrogen before storage at -80°C for later analysis.

Protein extraction and quantification for proteomics

Cell pellets were thawed on ice and bead beaten using lysing matrix B (MP Biomedicals, Irvine, CA) in buffer containing 50 mM HEPES pH 8.5, 1% SDS, and protease inhibitor cocktail (MilliporeSigma, P2714). A FastPrep-24 5G bead beating lysis system (MP Biomedicals) was used with a speed of 4 m s^{-1} for two 30 s cycles. Cellular debris was then removed by centrifugation at 16,000 g for 5 min. As the proteomic sample processing method used in this study is sensitive to interference by genomic DNA released during cell lysis, cell extracts were next incubated for 25 min at 4°C with end-over-end rotation in the presence of 500 units mL^{-1} Benzonase nuclease (MilliporeSigma, E1014). A small volume of each sample was then

removed for protein quantification before 10 mM dithiothreitol (DTT) was added to the remaining lysate. Samples were frozen at -80°C for later analysis.

Total protein concentrations were determined in duplicate for each sample using the Micro BCA protein assay kit (Thermo Scientific, 23235) following the manufacturers specifications. Diatom stoichiometric ratios of cellular carbon and nitrogen to protein content (Lourenço *et al.*, 1998; Lourenço *et al.*, 2004) were used along with measured cell densities and cell biovolumes to estimate the expected protein yield from each sample. Quantified total protein concentrations were compared to these estimates and reported as protein extraction efficiencies in Table S2. The four samples within each treatment with the highest extraction efficiencies were selected for proteomic sequencing. Proteomic sample preparation following the SP3 method (Hughes *et al.*, 2014) and LC-MS/MS sequencing were completed by staff at the Biological Mass Spectrometry Facility of Robert Wood Johnson Medical School and Rutgers, The State University of New Jersey (see supplemental *Proteomic sample processing* for details).

Proteomic data analysis and statistics

LC-MS/MS output files were produced in Thermo .raw format and were processed using DIA-NN ver. 2.0.2 (Demichev *et al.*, 2020; Kistner *et al.*, 2023, Preprint). In silico spectral library preparation began with curating available protein sequences from UniProt for *T. pseudonana*, which yielded 11,661 unique protein entries (see supplemental *In silico spectral library preparation* for details). These sequences were then used in conjunction with a universal contaminants library (Frankenfield *et al.*, 2022) to generate the in silico spectral library needed for protein identification and quantification. For the sample analysis run, the high precision Quant UMS quantification strategy was used with match between runs (MBR) enabled, protein

inference enabled, and the precursor false discovery rate (FDR) set to 1%. The main output report was then imported into R ver. 4.4.1 (R Core Team, 2024) for strict quality control filtering before robust ridge regression model fitting using the MSqRob2 Bioconductor R package ver. 1.12.0 (Goeminne *et al.*, 2016; Goeminne *et al.*, 2020; Sticker *et al.*, 2020). The full list of DIA-NN settings and filters are provided in the supplemental section *Data analysis with DIA-NN*. All pairwise comparisons between the LCHpH and HCLpH treatments and the LCHpH and LCLpH treatments were evaluated using the Benjamini-Hochberg method to control FDR (Tables S5 and S6). Differential protein abundances greater than 1.30-fold with an adjusted $P < 0.05$ were considered significant.

Predicted localizations of key proteins

Sequence analysis to explore the specific mitochondrial association of PEPC2 was completed using DeepLoc 2.1 set to high quality (slow) and long output (Ødum *et al.*, 2024). ASAFind 2.0 (Almagro Armenteros *et al.*, 2019; Gruber *et al.*, 2025) was used to reassess the predicted chloroplast localization of the one form of PYC detected in this study as it was specifically developed for use in diatoms.

Results

Culture conditions and growth

Extensive testing was conducted to achieve suitable pH control of experimental cultures (n=13-15 per treatment, data not shown). The first iteration of the experimental apparatus mixed each acid addition with laboratory air, which led to deviations in pH below the set point for both

low pCO_2 treatments. This variability likely resulted from greater headspace pCO_2 compared to the target level. LCHpH test cultures experienced average decreases of 0.08 ± 0.02 pH units (20.2 ± 4.7% increase in acidity) while LCLpH test cultures saw greater deviations, with an average decrease of 0.21 ± 0.13 pH units (62.2 ± 34.9% increase in acidity). Comparatively, pH in the HCLpH test cultures remained more stable (7.59 ± 0.05 pH units). Revising the apparatus so that cultures were mixed via pCO_2-matched gas mixtures improved the pH control of each treatment. This refined pH control system consistently maintained pH across all replicate cultures within each treatment group (Tables 1 and S1), where the average pH improved to 8.45 ± 0.02 for the LCHpH treatment, 7.60 ± 0.01 for the HCLpH treatment, and 7.58 ± 0.03 for LCLpH treatment. This comparison to preliminary data is reported to illustrate the difficulty of controlling pH, which will be revisited in the discussion.

Using the revised apparatus, growth rates were similar to maxima for *T. pseudonana* grown at 18°C under 24 h high-intensity light (Guillard and Ryther, 1962; Guillard 1975; Thompson *et al.*, 1990; Brown *et al.*, 1996; Thompson 1999; Parker and Armbrust, 2005; Laws *et al.*, 2020), with observed average growth rates of 1.98 ± 0.07 d^{-1}, 2.00 ± 0.08 d^{-1}, and 2.03 ± 0.08 d^{-1} for the LCHpH, HCLpH, and LCLpH treatments, respectively (Table 1). Variability in growth rates were similar across experimental conditions (Tables 1 and S2), indicating that the experimental apparatus did not disproportionately affect any one treatment.

Proteomic analysis overview

In total, 8,571 proteins were identified with a global false discovery rate of 1%. After quality control filtering, 7,803 accurately quantified proteins remained for further analysis. The comparison of the LCHpH and HCLpH conditions revealed 118 differentially abundant proteins

(> 1.30-fold change, adjusted $P < 0.05$), of which 72 were more abundant while 46 were less abundant in the LCHpH condition compared to the HCLpH condition (Fig. 1 and 2a, Table S3). Twelve differentially abundant proteins were found when comparing the LCHpH and LCLpH conditions, with 6 each more abundant in the LCHpH and LCLpH conditions, respectively (Fig. 2b, Table S4). When identifying differentially abundant proteins common to both low pH treatments, two uncharacterized proteins were found that were more abundant at low pH compared to high pH. Proteins will be referred to by their name and/or Uniprot ID throughout the remainder of this results section.

Differential abundance of proteins involved in carbon concentrating mechanisms

Seven annotated CAs were differentially abundant between the LCHpH and HCLpH conditions alongside an eighth possible CA (B8LE18; Table 2). δCA1, θCA1, θCA2, θCA3, and ζCA1 were more abundant in cells grown in the LCHpH condition, with respective fold increases of 5.10, 2.39, 1.40, 1.75, and 9.69. αCA3 and θCA4 were less abundant in cells from the LCHpH condition by 1.35- and 3.57-fold, respectively. γCA1, γCA4, and γCAL were also quantified in the LCHpH and HCLpH conditions, and no differences were detected. No differences in the abundance of any CA were found when comparing the low pCO_2 treatments.

In conjunction with CAs, HCO_3^- transport proteins can be important to CCMs as they facilitate the movement of HCO_3^- between subcellular compartments. Two known solute carrier family 4 (SLC4) HCO_3^- transporters, SLC4-1 (B8C6G1) and SLC4-2 (B8BQU6), have been identified in *T. pseudonana* (Nakajima *et al.*, 2013), but no differences in their abundances were detected (Tables S5 and S6). Additionally, two anion transporters that may be capable of moving HCO_3^-, bestrophin 1 and 2 (Nigishi *et al.*, 2024), were more abundant, by 2.09- and 2.81- fold,

respectively, in the LCHpH condition compared to the HCLpH condition (Table 2). The abundance of these bestrophins did not differ significantly between the low pCO_2 treatments.

Regardless of its source, HCO_3^- is required by PEPC to produce OAA. The abundance of PEPC1 did not vary significantly between treatments, although it did show an upward trend in LCHpH cells compared to HCLpH cells (1.26-fold increase, adjusted $P < 0.05$). PEPC2 was significantly more abundant (1.32-fold) under LCHpH compared to HCLpH conditions, and occurred alongside a 2.78-fold lower abundance of phosphoenolpyruvate carboxykinase (PEPCK), which catalyzes the inverse reaction of PEPC (Table2). While PEPC2 is referred to as the mitochondrial form of PEPC, current predictive localization tools can now provide deeper insight. DeepLoc 2.1 (Ødum *et al.*, 2024) predicts a general mitochondrial localization probability of 0.80 with a peripheral mitochondrial membrane association probability of 0.73, suggesting that PEPC2 is associated with the outer surface of mitochondria.

In the model C_4 plant CCM described above, OAA produced by PEPC is converted to malate by MDH. Three forms of MDH were quantified in this study, but only the abundance of the cytoplasmic form (MDH_c) varied significantly. The abundance of MDH_c (B5YNR1) was 1.55-fold higher in LCHpH cells compared to HCLpH cells (Table 2), with no difference detected between the LCHpH and LCLpH treatments.

The next step in a biochemical CCM would be for the newly formed malate to enter the chloroplast via carboxylate transporters. One such transporter is the 2-oxoglutarate/malate translocator (OMT), the abundance of which was similar between treatment groups. Characterizations of other carboxylate transporters are lacking in *T. pseudonana*, preventing any further evaluation of this aspect of its CCM.

Malate, once inside the chloroplast, can be decarboxylated by ME to release CO_2 near RuBisCO. The abundance of NAD^+-dependent ME (NAD-ME, W8VUB7) did not differ significantly between treatments and no other forms of ME have yet been identified in *T. pseudonana*. That said, a NAD(P)-binding domain-containing protein (B8LBP8) that shares its closest identity match (66.3%, Uniprot blast tool) with a short-chain dehydrogenase/reductase (SDR) family oxidoreductase in *Skeletonema marinoi* was 1.33-fold more abundant in cells grown in the LCHpH condition compared to the HCLpH condition. Alternatively, it has been hypothesized that pyruvate carboxylase (PYC) may serve as the decarboxylase in the stroma of *T. pseudonana* (Kustka *et al.*, 2014). Of the three known forms of PYC within *T. pseudonana*, only the form with a predicted plastidial localization (Kustka *et al.*, 2014; ASAFind 2.0 predicts a chloroplast signal peptide with high confidence) was accurately quantified here. Changes in the abundance of this PYC (B8CE42) did not cross the *a priori* protein fold-change significance threshold for either treatment comparison (Table S5 and S6).

After CO_2 has been released near RuBisCO, the regeneration of PEP from pyruvate produced during the decarboxylation of malate by ME, or OAA by PYC, would serve to resupply PEPC in the cytoplasm. This conversion can be catalyzed by pyruvate, phosphate dikinase (B8C332) and pyruvate, water dikinase (B8C779); however, neither protein was accurately quantified in this study.

Differential abundance of proteins in alternative pathways employing the malate/OAA shuttle

The pH homeostasis pathways described by Sakano (1998) rely on several enzymes that may also be involved in the CCM of *T. pseudonana*. The first step described in response to elevated intracellular pH is to increase PEPC activity, which aligns with the observed 1.32-fold

increase in PEPC2 abundance in LCHpH cells compared to HCLpH cells. When testing the effect of pH alone, no difference in PEPC2 abundance was detected between the LCHpH and LCLpH conditions. Looking further downstream in this pathway, increased PEPC activity consumes PEP, which removes inhibition on phosphofructokinase allowing glycolytic reactions to proceed that yield net H^+ ions. No significant differences in abundance were detected in any form of phosphofructokinase and furthermore, no differences were observed in the five detected forms of pyruvate kinase, an enzyme also capable of consuming PEP (Table S5 and S6).

The complementary side of this pH homeostasis mechanism that functions as a proton sink relies on NAD-ME to supply NADH + H^+ into the alternative respiratory pathway. No differences were detected among the three treatments for the only known form of NAD-ME (W8VUB7) in *T. pseudonana*. Downstream of ME, this pH regulatory pathway is dependent upon mitochondrial alternative oxidases (AOX) to transfer protons from NADH + H^+ to molecular oxygen, reducing it to water (see reviews by Selinski and Scheibe, 2018; Chadee *et al.*, 2021). No significant differences in the abundance of either AOX1 (B8CF37) or AOX2 (B8CF38) were found (Table 2). A non-electrogenic form of mitochondrial electron transport chain complex I (B8LBH6), which when paired with AOX can facilitate the oxidation of NADH + H^+ without altering cellular energy balance, was also detected and no significant differences in its abundance were observed. Although not described in Sakano (1998), the alternative oxidases within the chloroplast, which function similarly to AOX while utilizing NADPH + H^+, could also act as a proton sink when working in conjunction with the malate/OAA shuttle. While plastidial terminal oxidase 1 (PTOX1, B8CC74) could not be quantified, no variations in the abundance of PTOX2 (B8LD44) were observed (Table 2).

Another cellular mechanism that can involve the malate/OAA shuttle is cyclic electron transport around photosystem I (CET; reviewed in Chadee *et al.*, 2021). The two known pathways of CET are dependent on 1) the proton gradient regulation 5 protein (PGR5, B8C035) in conjunction with the PGR5-like photosynthetic phenotype 1 protein (PGRL1, B8BZQ3) and 2) the NADH-like (NDH) complex. No significant differences in the abundances of PGR5 and PGRL1 were detected (Table 2), and while numerous subunits are known to comprise the NDH complex in *T. pseudonana*, many remain poorly characterized making its evaluation difficult.

Discussion

The proteomic analysis resulted in 7,803 quantified proteins following rigorous filtering. This represents one of the most complete *T. pseudonana* proteomes to date, and therefore, allowed for an in-depth exploration of both the CCM and other metabolic pathways that could produce similar protein abundance profiles. Differential protein abundances are discussed in a stepwise fashion proceeding through the proposed CCM of *T. pseudonana* (Fig. 3). This is followed by a discussion of intracellular CO_2 recapture (Fig. 4) before alternative explanations for increased abundances of C_4 CCM enzymes are evaluated. This section concludes with an examination of challenges inherent to exploring the CCM of *T. pseudonana* and strategies to avoid them moving forward.

Carbon concentrating mechanism

Step 1: Extracellular DIC uptake

CCMs must begin with the uptake of extracellular DIC in the form of CO_2 or HCO_3^-, which can be facilitated by externally acting CAs and HCO_3^- transporters (reviewed by Reinfelder *et al.*, 2011). TpδCA1 and TpζCA1 are both believed to operate in the periplasmic space (Tachibana *et al.*, 2011; Samukawa *et al.*, 2014; Hopkinson *et al.*, 2016) and showed two of the largest increases in protein abundance in LCHpH compared to HCLpH conditions (Table S3). The upregulation of external CAs to produce HCO_3^- would seemingly be of little benefit if HCO_3^- uptake is the initial step of the CCM, as the total DIC pool at both pH 7.61 and 8.48 is predominantly HCO_3^- (Mehrbach *et al.*, 1973; Dickson and Millero, 1987; Lueker *et al.*, 2000). Furthermore, recent work has shown that *T. pseudonana* is insensitive to a known inhibitor of extracellular SLC4 family HCO_3^- transporters while exposure to an extracellular CA inhibitor produced a marked decrease in its affinity for DIC (Tsuji *et al.*, 2017). The current study found no significant changes in the abundance of any potential extracellular HCO_3^- transporter or ATPase, at least a pair of which would be needed to facilitate increased HCO_3^- uptake (Thielmann *et al.*, 1990; Karlsson *et al.*, 1994; Nakajima *et al.*, 2013; Wang *et al.*, 2015; Poschenrieder *et al.*, 2018; Nawaly *et al.*, 2023a). Taken together, these results further solidify the first step of the CCM in *T. pseudonana* as the passive influx of CO_2 generated by external CA activity (Moroney *et al.*, 2011; Hopkinson *et al.*, 2013; Kustka *et al.*, 2014; Tsuji *et al.*, 2017; Tsuji *et al.*, 2021).

Step 2: The role of cytoplasmic carbonic anhydrases

The next logical step would be the "capture" of CO_2 entering the cell through its CA-mediated conversion back to HCO_3^- to prevent diffusive losses. Two cytosolic forms of CA, TpαCA3 and TpθCA4 (Tachibana *et al.*, 2011; Nawaly *et al.*, 2023b), were differentially

abundant in this study; however, they were more abundant in the HCLpH compared to the LCHpH condition. As CAs can serve dual roles to both concentrate DIC and regulate cellular acid-base status, contrasting interpretations must be considered (Reinfelder *et al.*, 2011; Supuran, 2016; Occhipinti and Boron, 2019). Increased abundances of TpαCA3 and TpθCA4 at high pCO_2 could indicate that these CAs act to buffer cytoplasmic acidification driven by the greater influx of CO_2 (Badger and Price, 1994; Occhipinti and Boron, 2019). This would not preclude them from converting influxing CO_2 to HCO_3^- under low pCO_2 conditions, but instead could simply indicate that they are needed in greater abundance for acid-base regulation at a pCO_2 of 1702 μatm compared to that needed for CO_2 capture at a pCO_2 of 202 μatm. Conversely, decreased abundances of TpαCA3 and TpθCA4 in response to low pCO_2 would negate their involvement in the CCM. The totality of low pCO_2-induced changes in protein abundances when considered with the lack of corresponding changes in HCO_3^- uptake mechanisms; however, suggest that *T. pseudonana* relies on cytoplasmic CAs to convert influxing CO_2 to HCO_3^- at both tested pCO_2 levels.

Step 3: OAA formation

PEPC2 abundance in *T. pseudonana* increased in response to low pCO_2 but not extracellular pH, indicating that it could serves as a C_4 carboxylase in the CCM. As current predictions for *T. pseudonana*, which concur with observations in other phototrophs (O'Leary *et al.*, 2011; Park *et al.*, 2012; O'Leary and Plaxton, 2020), place PEPC2 on the peripheral surface of the mitochondria, it likely utilizes cytoplasmic pools of PEP and HCO_3^- to produce OAA. This localization still allows PEPC2 to serve in its anaplerotic role for the TCA cycle through coupling with known mitochondrial dicarboxylate transporters (O'Leary *et al.*, 2011; Park *et al.*,

2012; Schober *et al.*, 2019; Fernie *et al.*, 2020; Liu *et al.*, 2022; Zara *et al.*, 2022) while also preventing the futile cycling of OAA through the spatial isolation of PEPC2 and PEPCK (Kustka *et al.*, 2014). The observed decrease in PEPCK abundance under low pCO_2 conditions would further support maximal CCM functioning by reducing OAA demand within the mitochondria. While more work is needed to confirm the localization of PEPC2, there is another discovery pertaining to both PEPC1 and PEPC2 that could have major implications for past findings on the role of PEPC in the CCM of *T. pseudonana*.

Work in green algae and land plants has revealed the existence of a heteromeric PEPC complex (termed the class 2 PEPC complex), composed of four subunits each of PEPC1 and PEPC2, that may be the only form in which PEPC2 subunits function within these taxa (Rivoal *et al.*, 1996; Rivoal *et al.*, 1998; Rivoal *et al.*, 2002; Mamedov *et al.*, 2005; Moellering *et al.*, 2007; O'Leary *et al.*, 2011; Park *et al.*, 2012; Ting *et al.*, 2017; Koendjbiharie *et al.*, 2021; Hu *et al.*, 2025). This complex is localized to the surface of the mitochondria and is less sensitive, relative to homotetrameric PEPC1 complexes, to allosteric inhibition by metabolic intermediates, such as malate and aspartate (O'Leary *et al.*, 2009; O'Leary *et al.*, 2011; Park *et al.*, 2012; Ting *et al.*, 2017). As will be discussed more fully below, malate likely plays a central role in the biochemical aspects of the CCM in *T. pseudonana*, and therefore, the presence of a malate-resistant PEPC complex would help to facilitate optimal CCM functioning. If the presence of a class 2 PEPC complex in *T. pseudonana* is verified, it would call for a reexamination of previously reported PEPC data. Parallel increases in both PEPC1 and PEPC2 (Granum *et al.*, 2009; Kustka et al 2014) could be indicative of the upregulation of the hybrid class 2 complex. While the change observed here in PEPC1 abundance did not cross the *a priori* protein fold change significance threshold, the 1.26-fold (adjusted P = 0.001) increase under LCHpH

compared to HCLpH conditions is similar to the 1.32-fold increase in PEPC2 abundance, which would align with increased demand for the class 2 complex. Additionally, careful consideration of PEPC activity measurements would be warranted, as active class 2 complexes have proven difficult to extract given their high susceptibility to cleavage by thiol endopeptidases (Blonde and Plaxton, 2003; Gennidakis *et al.*, 2007; O'Leary *et al.*, 2009). Although this remains speculative, it highlights the need for future work exploring the molecular structure of diatom PEPC complexes in order to fully understand the operation and regulation of their CCMs.

Step 4: Malate formation and transport

The abundance of MDH_c increased in response to low pCO_2 conditions, but was unaffected by extracellular pH, suggesting that OAA is reduced to malate in the cytosol before it is translocated into the chloroplast stroma. Malate exchange across the chloroplast envelope can readily occur as several plastidial di- and tri- carboxylate transporters (e.g. OMT, DiT2) are less substrate specific than initially believed (Taniguchi *et al.*, 2002; Kinoshita *et al.*, 2011; Selinski and Scheibe, 2018). While no change in the abundance of OMT was detected, and no increase in any transporter may be necessary if malate translocation occurs rapidly, more work is needed to characterize other plastidial carboxylate transporters in *T. pseudonana* as few are well described.

Step 5: Decarboxylation near RuBisCO

In the simplest C_4 plant CCM, $NADP^+$-dependent malic enzyme (NADP-ME) decarboxylates malate back to pyruvate while releasing CO_2 (reviewed by Leegood, 2002). The only annotated ME in *T. pseudonana* showed similar abundances across all treatment groups in this study and to date, no forms of NADP-ME or additional forms of NAD-ME have been

observed (Tanaka *et al.*, 2014; Davis *et al.*, 2017). However, an NAD(P)-binding domain-containing protein (B8LBP8) was significantly more abundant in cells grown under low pCO_2 (Table 2). Uniprot blast tool results showed that its closest identity match is to an SDR family NAD(P)-dependent oxidoreductase (A0AAD8Y4P9) found in another centric diatom, *S. marinoi*. While the SDR family of oxidoreductases contains thousands of proteins, it is the family within which ME resides (Kavanagh *et al.*, 2008; Moon *et al.*, 2012; Tronconi *et al.*, 2018). The NAD(P)-binding domain of B8LBP8 encapsulates all but 29 of its amino acids with no other known domains detected (NCBI conserved domain search tool, Marchler-Bauer *et al.*, 2017; Lu *et al.*, 2020; Wang *et al.*, 2023), indicating that this protein sequence may be incomplete. While this by no means identifies the decarboxylase in the CCM of *T. pseudonana*, it does provide a direction for future research into uncharacterized oxidoreductases that may not be fully represented in the current reference genome.

Alternatively, it has been proposed that PYC could serve as the final decarboxylase within *T. pseudonana* (Kustka *et al.*, 2014). In this scenario, OAA is transported into the stroma instead of malate where its subsequent decarboxylation by PYC releases CO_2. The only form of PYC detected in this analysis has a predicated localization to the chloroplast, and while there was an increasing trend in its abundance in the LCHpH condition compared to the HCLpH condition, this was not significant. Given the previously reported increase in this PYC under low CO_2 conditions (Kustka *et al.*, 2014) and the two forms of PYC that could not be quantified here, a more targeted assessment of the role of PYC in the CCM of *T. pseudonana* may be warranted. However, if PYC is the stromal decarboxylase, the role of MDH_c would need to be reevaluated as it would seemingly limit CCM functioning by reducing the availability of cytosolic OAA (reviewed in Selinski and Scheibe, 2018).

Step 6: Crossing the pyrenoid protein shell

Recent advancements localizing the θCAs and resolving the pyrenoid ultrastructure in *T. pseudonana* have helped to elucidate the most likely final steps of the CCM within the chloroplast (Nawaly *et al.*, 2023b; Nam *et al.*, 2024; Shimakawa *et al.*, 2024). The abundances of two stromal θCAs, TpθCA1 and TpθCA3, increased in response to low pCO_2 conditions, but were unaffected by extracellular pH. It has been hypothesized that one or both of these CAs act to recapture CO_2 that escapes the pyrenoid-penetrating thylakoid (PPT; Nawaly *et al.*, 2023b); however, here it is proposed that they primarily serve to convert CO_2 released from the decarboxylation of malate into HCO_3^-. Morphological similarities between prokaryotic carboxysomes and the pyrenoid protein shell of *T. pseudonana* suggest that the pyrenoid could be impermeable to CO_2 (Nam *et al.*, 2024; Shimakawa *et al.*, 2024), which would reduce the need for a dedicated CO_2 recapture mechanism in the stroma. Once TpθCA1 and TpθCA3 capture CO_2 released from the decarboxylation of malate, the resultant HCO_3^- needs to pass into the PPT lumen where the final step of the CCM resides. Bestrophin 1 and 2, which have recently been localized to the PPT membrane in *T. pseudonana* (Nigishi *et al.*, 2024), could facilitate this movement as bestrophins are known to be permeable to HCO_3^- (Qu and Hartzell, 2008). Furthermore, the passage of HCO_3^- through bestrophin channels into the PPT lumen has been documented in several other marine algae (Mukherjee *et al.*, 2019; Nigishi *et al.*, 2024). This function is similarly supported in *T. pseudonana* as the abundances of bestrophin 1 and 2 increased in response to low pCO_2 in both this study and others (Kustka *et al.*, 2014; Nigishi *et al.*, 2024).

Step 7: Dehydration of HCO_3^-

TpθCA2 has been localized within the PPT, where it likely converts stroma-derived HCO_3^- to CO_2 that then diffuses to RuBisCO in the interior of the pyrenoid (Nawaly *et al.*, 2023b; Nam *et al.*, 2024; Shimakawa *et al.*, 2024). This role is supported here as TpθCA2 abundance increased in response to low pCO_2, but was insensitive to changes in external pH. While several key areas still require additional characterization, taken as a whole, the results presented here are consistent with a hybrid CCM in *T. pseudonana* that consists of both biophysical and biochemical steps working in unison to supply CO_2 to RuBisCO.

Intracellular CO_2 recapture mechanism

Several CA-mediated recapture mechanisms of respired CO_2 have been proposed for *T. pseudonana* (Trimborn *et al.*, 2009; Tachibana *et al.*, 2011; Samukawa *et al.*, 2014; Nawaly *et al.*, 2023b). However, the strongest case for recycling involves γCA-mediated recapture of CO_2 from the TCA cycle (Fig. 4; Cardol *et al.*, 2004; Parisi *et al.*, 2004; Mitra *et al.*, 2005; Perales *et al.*, 2005; Sunderhaus *et al.*, 2006; Braun and Zabaleta, 2007; Zabaleta *et al.*, 2012; Soto *et al.*, 2015; Fromm *et al.*, 2016a; Fromm *et al.*, 2016b; Cainzos *et al.*, 2021; Klusch *et al.*, 2023; Maldonado *et al.*, 2023; Braun and Klusch, 2024). Structural analyses in other phototrophs have shown that γCAs and γCA-like proteins (γCAL) form a domain within complex I of the mitochondrial electron transport chain (ETC) that protrudes into the mitochondrial matrix (Sunderhaus *et al.*, 2006; Meyer *et al.*, 2011; Klusch *et al.*, 2023; Maldonado *et al.*, 2023) where it converts CO_2 to HCO_3^-. This γCA domain has not been found to function freely of complex I (Martínez-Reyes and Chandel, 2020; Cainzos *et al.*, 2021; Klusch *et al.*, 2023; Maldonado *et al.*, 2023; Braun and Klusch, 2024), indicating that the cellular demand for complex I likely dictates

its expression. Recent work in *T. pseudonana* has shown that γCA1, γCA4, and γCAL are capable of forming a heterotrimeric domain with a functional active site (Cainzos *et al.*, 2021). The abundance profiles of these γCA subunits and other complex I components were similar among the treatment groups assessed here, which is consistent with this mechanism. A mitochondrial CA-dependent recapture mechanism has been previously considered in algae and was suggested to be energetically favorable. Specifically, Raven (2001) hypothesized that HCO_3^- channels could exist in the mitochondrial membranes of algae to move recaptured DIC without the risk of CO_2 leakage. It was estimated that these HCO_3^- channels could increase the supply of CO_2 to RuBisCO by 10% at a cost of <1% of total cellular ATP production. To date, few HCO_3^- channels are known in *T. pseudonana* (Nakajima *et al.*, 2013; Tsuji *et al.*, 2017) and localization studies are lacking, so more work is needed to further evaluate this recapture mechanism.

Evidence for alternative cellular pathways employing similar machinery

The quantitative proteomic analysis of *T. pseudonana* allowed for the evaluation of whether the observed upregulation of PEPC and MDH_c were driven by demand for the CCM or instead by increased demand for the transport of reducing equivalents via the malate/OAA shuttle. This shuttle in conjunction with the alternative oxidases, which act as shunts that uncouple electron transport to preserve redox poise at the cost of ATP production, can be involved in pH homeostasis, cyclic electron transport, and excess energy dissipation (Shikanai, 2007; Yoshida *et al.*, 2007; van Dongen *et al.*, 2011; Yu *et al.*, 2014; Nawrocki *et al.*, 2015; Dietz *et al.*, 2016; Murik *et al.*, 2018; Chadee *et al.*, 2021; Zhou *et al.*, 2021; Hippmann *et al.*, 2022; Degen *et al.*, 2024). Studies have shown that the alternative oxidases are active in cellular

functions ranging from respiration to stress tolerance, with correspondingly complex regulatory pathways tightly controlling their expression (Yoshida *et al.*, 2007; van Dongen *et al.*, 2011; Nawrocki *et al.*, 2015; Murik *et al.*, 2018; Vanlerberghe *et al.*, 2020).

When evaluating the possible involvement of the previously described pH homeostasis pathways (Sakano, 1998), the lack of changes in the abundances of both AOX and PTOX between either low pH treatment and the high pH treatment indicates that the pathway to reduce intracellular H^+ concentration was not upregulated at an extracellular pH of 7.61. There was also no sign that the H^+ generating pathway was active in cultures grown at pH 8.48 as no changes in PEPC abundance were detected between the LCHpH and LCLpH groups.

The malate/OAA shuttle is also known to support some forms of cyclic electron transport (CET) around photosystem I (Shikanai, 2007; Nawrocki *et al.*, 2015; Chadee *et al.*, 2021). CET on its own circumvents NADPH + H^+ production while still producing ATP to help correct energy imbalances caused by increased ATP consumption. When paired with either PTOX or AOX via the malate/OAA shuttle, CET aids in $NADP^+$ regeneration, thereby maintaining both energy balance and redox poise within the chloroplast (Yamori *et al.*, 2015; Chadee *et al.*, 2021). Of the two known CET pathways, the PGR5 pathway and the NDH pathway (Yamori *et al.*, 2015; Chadee *et al.*, 2021; Zhou *et al.*, 2021; Degen *et al.*, 2024), PGR5-dependent CET is more well characterized in *T. pseudonana*. No proteins uniquely involved in this pathway were differentially abundant in this study, and while the NDH pathway is not fully characterized in *T. pseudonana*, there was no indication of differential abundance of any suspected NDH complex subunit (Tables S5 and S6). When considered in conjunction with the lack of changes in AOX and PTOX, there is no evidence that CET is responsible for the results obtained in this study.

Lastly, a mechanism for dissipating excess light energy while combating oxidative stress that relies on the non-electrogenic homolog of mitochondrial complex I, the malate/OAA shuttle, and AOX was examined (Selinski and Scheibe, 2018). In addition to the lack of differences in the AOXs and the non-electrogenic form of complex I, no indications of elevated oxidative stress (e.g. more abundant superoxidase dismutase, catalase, glutathione peroxidase, glutathione reductase; Tables S5 and S6) were observed, demonstrating that this energy dissipation mechanism is not differentially active among treatments. Overall, no evidence of any alternative mechanism was found that could detract from the conclusion that PEPC and MDH_c are active in the CCM of *T. pseudonana*.

Experimental challenges and strategies moving forward

Achieving stringent pH control in all treatments required extensive testing and a refined experimental apparatus. pH control is critical as *T. pseudonana* exhibits rapid changes in carbon metabolism in response to changes in pH and pCO_2. (Roberts *et al.*, 2007; Granum *et al.*, 2009; Kustka *et al.*, 2014; Clement *et al.*, 2016; Clement *et al.*, 2017). That said, some *T. pseudonana* CCM studies provide little to no quantification of the carbonate chemistry within their experimental cultures (Table 3), making true comparisons between them challenging. Maintaining consistent carbonate chemistry conditions has proven difficult when diatom cultures are grown to high biomass (Shi *et al.*, 2009; Crawfurd *et al.*, 2011); however, the specific design of an experimental apparatus can also lead to poorly controlled carbonate chemistry at even low biomass, as was reported here for the preliminary experimental setup. While the lack of carbonate chemistry monitoring does not necessarily indicate that culture conditions were poorly

maintained, large deviations from well-established growth rates are more suggestive of the influence of unknown factors.

As growth is a widely used metric to assess the health of algal cultures, many studies have measured growth rates of *T. pseudonana* (CCMP 1335; previously clone 3H) across a range of temperatures, light conditions, and nutrient concentrations (Guillard and Ryther, 1962; Guillard *et al.*, 1973; Guillard, 1975; Thompson *et al.*, 1990; Brown *et al.*, 1996; Thompson 1999; Parker and Armbrust, 2005; Shi *et al.*, 2015; Laws *et al.*, 2020). This body of work has shown that nutrient replete *T. pseudonana* cultures grown between 15 and 20°C with continuous low-intensity light (~50 μmol photon m^{-2} s^{-1}) should exhibit a minimum growth rate of approximately 1.5 d^{-1} (2.2 divisions d^{-1}). Similar cultures grown with higher intensity light (> 150 μmol photon m^{-2} s^{-1}) should achieve growth rates from 1.8 d^{-1} to as high as 2.3 d^{-1} (2.6 and 3.3 divisions d^{-1}, respectively). While some variability is expected across studies, large deviations from these values are likely indicative of confounding variables adversely affecting *T. pseudonana*. Studies reporting lower than expected growth rates as well as those where growth is not reported are common in the *T. pseudonana* CCM literature (Table 3). Comparing studies with growth rates that deviate to varying degrees from well characterized expectations can lead to inadvertently erroneous conclusions. To ensure new findings are properly contextualized, all physiological studies should report calculated growth rates moving forward.

In the present study, high and low pCO_2 *T. pseudonana* cultures were maintained under conditions that yielded maximal growth rates (Guillard and Ryther, 1962; Thompson 1999; Parker and Armbrust, 2005; Laws *et al.*, 2020). As cellular carbon demand is predicated on growth, maximally growing low pCO_2 cultures would have the greatest need for elevated CCM expression. This approach was implemented over the use of extreme CO_2 levels (from 50 to

20,000 ppm; Clement *et al.*, 2016; Clement *et al.*, 2017; Jensen *et al.*, 2019; Nawaly *et al.*, 2023b; Nigishi *et al.*, 2024) as using levels that far exceed those experienced in the evolutionary history of diatoms could produce physiological responses unrelated to the CCM (Kuhn and Kasting, 1983; Kasting, 1993; Kah and Riding, 2007; Feulner, 2012; Novák Vanclová and Dorrell, 2024). To accurately interpret results generated using extreme CO_2 conditions, evidence from additional intermediate CO_2 levels is needed to ensure observed responses are representative of CCM functioning alone. It is therefore suggested that future studies employ more reasonable pCO_2 levels to alleviate the need for expansive factorial designs and to provide added insights into how this species will respond to projected future changes in ocean carbonate chemistry.

Conclusion

The proteomic data presented in this study demonstrate strong evidence for a hybrid CCM within *T. pseudonana*. These results agree with recent work that both the initial and final steps of the CCM are biophysical, while the intermediate steps rely on C_4 intermediates to translocate CO_2 near to RuBisCO. Future investigations into the identity and structure of the PEPC complexes present within *T. pseudonana*, the identity of the stromal decarboxylase, and the potential presence of mitochondrial HCO_3^- channels will provide clarity on the as yet unelucidated steps within this CCM. The proteomic approach used here also provided the first in-depth evaluation of alternative pathways reliant upon the malate/OAA shuttle within *T. pseudonana* and found no evidence of any such mechanism that could account for changes in CCM enzymes, as had been previously suggested. Continued study of diatom CCMs will serve to not only improve the understanding of how ongoing climate change and ocean acidification

will impact these key primary producers, but it will also support emerging interests into their biotechnological applications.

Supplementary data

The following supplementary data are available at JXB online.

Table S1. Average pH_{NBS} for each treatment replicate.

Table S2. Growth rates and protein extraction efficiencies for all experimental cultures.

Table S3. List of all differentially abundant proteins for the LCHpH and HCLpH comparison.

Table S4. List of all differentially abundant proteins for the LCHpH and LCLpH comparison.

Table S5. Full statistical output for the LCHpH and HCLpH comparison.

Table S6. Full statistical output for the LCHpH and LCLpH comparison.

Supplemental information: Detailed laboratory procedures, experimental apparatus construction, and extended lists of software settings.

Acknowledgments

The authors thank David Sleat, Haiyan Zheng, and Amenah Soherwardy for their expertise in completing proteomic sample preparation and LC-MS/MS protein sequencing, and for advising on the ensuing data analysis.

Author contributions

ABK: conceptualization; ABK: funding acquisition; ARH and ABK: methodology; ABK and ARH: investigation; ARH: formal analysis; ARH: data curation; ARH: writing - original draft; ABK and ARH: writing - review & editing; ARH: visualization; ABK: supervision.

Conflict of interest

No conflict of interest declared.

Funding

This work was supported by the Rutgers University Core Facilities Utilization Grant Program and Rutgers University-Newark Initiative for Multidisciplinary Research Teams Program to ABK.

Data availability

The raw mass spectrometry files and DIA-NN main report file have been deposited to the ProteomeXchange Consortium (http://proteomecentral.proteomexchange.org) via the PRIDE partner repository (Perez-Riverol *et al.*, 2025) with the dataset identifier PXD064793.

References

Almagro Armenteros JJ, Salvatore M, Emanuelsson O, Winther O, von Heijne G, Elofsson A, Nielsen H. 2019. Detecting sequence signals in targeting peptides using deep learning. Life Science Alliance. 2, e201900429.

Alverson AJ, Jansen RK, Theriot EC. 2007. Bridging the Rubicon: phylogenetic analysis reveals repeated colonizations of marine and fresh waters by thalassiosiroid diatoms. Molecular Phylogenetics and Evolution. 45, 193-210.

Armbrust EV. 2009. The life of diatoms in the world's oceans. Nature. 459, 185-192.

Armbrust EV, Berges JA, Bowler C, *et al.* 2004. The genome of the diatom *Thalassiosira pseudonana*: Ecology, evolution, and metabolism. Science. 306, 79-86.

Behrenfeld MJ, Randerson JT, McClain CR, *et al.* 2001. Biospheric primary production during and ENSO transition. Science. 291, 2594-2597.

Blonde JD, Plaxton WC. 2003. Structural and kinetic properties of high and low molecular mass phosphoenolpyruvate carboxylase isoforms from the endosperm of developing castor oilseeds. The Journal of Biological Chemistry. 278, 11867-11873.

Bowler C, Allen AE, Badger JH, *et al.* 2008. The Phaeodactylum genome reveals the evolutionary history of diatom genomes. Nature. 456, 239-244.

Braun H-P, Klusch N. 2024. Promotion of oxidative phosphorylation by complex I-anchored carbonic anhydrases? Trends in Plant Science. 29, P64-71.

Braun H-P, Zabaleta E. 2007. Carbonic anhydrase subunits of the mitochondrial NADH dehydrogenase complex (complex I) in plants. Physiologia Plantarum. 129, 114-122.

Brown MR, Dunstan GA, Norwood SJ, Miller KA. 1996. Effects of harvest stage and light on the biochemical composition of the diatom *Thalassiosira pseudonana*. Journal of Phycology. 32, 64-73.

Cainzos M, Marchetti F, Popovich C, Leonardi P, Pagnussat G, Zabaleta E. 2021. Gamma carbonic anhydrases are subunits of the mitochondrial complex I of diatoms. Molecular Biology. 116, 109-125.

Cardol P, Vanrobaeys F, Devreese B, Van Beeumen J, Matagne RF, Remacle C. 2004. Higher plant-like subunit composition of mitochondrial complex I from *Chlamydomonas reinhardtii*: 31 conserved components among eukaryotes. Biochimica et Biophysica Acta. 1658, 212-224.

Chadee A, Alber NA, Dahal K, Vanlerberghe GC. 2021. The complementary roles of chloroplast cyclic electron transport and mitochondrial alternative oxidase to ensure photosynthetic performance. Frontiers in Plant Science. 12, 748204.

Clement R, Dimnet L, Maberly SC, Gontero B. 2016. The nature of the CO_2 -concentrating mechanisms in a marine diatom, *Thalassiosira pseudonana*. New Phytologist. 209, 1417-1427.

Clement R, Lignon S, Mansuelle P, Jensen E, Pophillat M, Lebrun R, Denis Y, Puppo C, Maberly SC, Gontero B. 2017. Responses of the marine diatom *Thalassiosira pseudonana* to changes in CO_2 concentration: a proteomic approach. Scientific Reports. 7, 42333.

Crawfurd KJ, Raven JA, Wheeler GL, Baxter EJ, Joint I. 2011. The response of *Thalassiosira pseudonana* to long-term exposure to increased CO_2 and decreased pH. PLOS ONE. 6, e26695.

Davis A, Abbriano R, Smith SR, Hildebrand M. 2017. Clarification of Photorespiratory Processes and the Role of Malic Enzyme in Diatoms. Protist. 168,134-153.

Degen GE, Pastorelli F, Johnson MP. 2024. Proton gradient regulation 5 is required to avoid photosynthetic oscillations during light transitions. Journal of Experimental Botany. 75, 947-961.

Demichev V, Messner CB, Vernardis SI, Lilley KS, Ralser M. 2020. DIA-NN: neural networks and interference correction enable deep proteome coverage in high throughput. Nature Methods. 17, 41-44.

Dickson AG, Millero FJ. 1987. A comparison of the equilibrium constants for the dissociation of carbonic acid in seawater media. Deep Sea Research Part A Oceanographic Research Papers. 34, 1733-1743.

Dickson AG, Wesolowski DJ, Palmer DA, Mesmer RE. 1990. Dissociation constant of bisulfate in aqueous sodium chloride solutions to 250°C. Journal of Physical Chemistry. 94, 7978–7985.

Dietz K-J, Turkan I, Krieger-Liszkay A. 2016. Redox- and reactive oxygen species-dependent signaling into and out of the photosynthesizing chloroplast. Plant Physiology. 171, 1541-1550.

Edwards GE, Franceschi VR, Voznesenskaya EV. 2004. Single-cell C_4 photosynthesis versus the dual-cell (Kranz) paradigm. Annual Review of Plant Biology. 55, 173-196.

Fernie AR, Cavalcanti JHF, Nunes-Nesi A. 2020. Metabolic roles of plant mitochondrial carriers. Biomolecules. 10, 1013.

Feulner G. 2012. The faint young Sun problem. Reviews of Geophysics. 50, RG2006.

Field CB, Behrenfeld MJ, Randerson JT, Falkowski P. 1998. Primary production of the biosphere: Integrating terrestrial and oceanic components. Science. 281, 237-240.

Frankenfield AM, Ni J, Ahmed M, Hao L. 2022. Protein Contaminants Matter: Building Universal Protein Contaminant Libraries for DDA and DIA Proteomics. Journal of Proteome Research. 21, 2104-2113.

Fromm S, Braun H-P, Peterhansel C. 2016a. Mitochondrial gamma carbonic anhydrases are required for complex I assembly and plant reproductive development. New Phytologist. 211, 194-207.

Fromm S, Senkler J, Zabaleta E, Peterhänsel C, Braun HP. 2016b. The carbonic anhydrase domain of plant mitochondrial complex I. Physiologia Plantarum. 157, 289-296.

Gastineau R, Hamedi C, Baba Hamed MB, *et al.* 2021. Morphological and molecular identification reveals that waters from an isolated oasis in Tamanrasset (extreme South of Algerian Sahara) are colonized by opportunistic and pollution-tolerant diatom species. Ecological Indicators. 121, 107104.

Gennidakis S, Rao S, Greenham K, Uhrig RG, O'Leary B, Snedden WA, Lu C, Plaxton WC. 2007. Bacterial- and plant-type phosphoenolpyruvate carboxylase polypeptides interact in

the hetero-oligomeric Class-2 PEPC complex of developing castor oil seeds. The Plant Journal. 52, 839-849.

Goeminne LJE, Gevaert K, Clement L. 2016. Peptide-level Robust Ridge Regression Improves Estimation, Sensitivity, and Specificity in Data-dependent Quantitative Label-free Shotgun Proteomics. Molecular & Cellular Proteomics. 15, 657-668.

Goeminne LJE, Sticker A, Martens L, Gevaert K, Clement L. 2020. MSqRob Takes the Missing Hurdle: Uniting Intensity- and Count-Based Proteomics. Analytical Chemistry. 92, 6278-6287.

Granum E, Raven JA, Leegood RC. 2005. How do marine diatoms fix 10 billion tonnes of inorganic carbon per year? Canadian Journal of Botany. 83, 898-908.

Granum E, Roberts K, Raven JA, Leegood RC. 2009. Primary carbon and nitrogen metabolic gene expression in the diatom *Thalassiosira pseudonana* (Bacillariophyceae): diel periodicity and effects of inorganic carbon and nitrogen. Journal of Phycology. 45, 1083-1092.

Gruber A, Vohnoutová M, McKay C, Rocap G, Oborník M. 2025. ASAFind 2.0: multi-class protein targeting prediction for diatoms and algae with complex plastids. The Plant Journal. 122, e70138.

Guillard RRL. 1975. Culture of phytoplankton for feeding marine invertebrates. In: Smith WL, Chanley MH (eds). Culture of marine invertebrate animals. Springer, Boston, MA.

Guillard RRL, Kilham P, Jackson TA. 1973. Kinetics of silicon-limited growth in the marine diatom *Thalassiosira pseudonana* Hasle and Heimdal (=*Cyclotella nana* Hustedt). Journal of Phycology. 9, 233-237.

Guillard RRL, Ryther JH. 1962. Studies of marine planktonic diatoms. I. *Cyclotella nana* Hustedt, and *Detonula confervacea* (Cleve) Gran. Canadian Journal of Microbiology. 8, 229-239.

Hennon GMM, Ashworth J, Groussman RD, Berthiaume C, Morales RL, Baliga NS, Orellana MV, Armbrust EV. 2015. Diatom acclimation to elevated CO_2 via cAMP signaling and coordinated gene expression. Nature Climate Change. 5, 761-765.

Hertle AP, Blunder T, Wunder T, Pesaresi P, Pribil M, Armbruster U, Leister D. 2013. PGRL1 is the elusive ferredoxin-plastoquinone reductase in photosynthetic cyclic electron flow. Molecular Cell. 49, 511-523.

Hippmann AA, Schuback N, Moon K-M, McCrow JP, Allen AE, Foster LF, Green BR, Maldonado MT. 2022. Proteomic analysis of metabolic pathways supports chloroplast-mitochondria cross-talk in a Cu-limited diatom. Plant Direct. 6, e376.

Hopkinson BM, Dupont CL, Matsuda Y. 2016. The physiology and genetics of CO_2 concentrating mechanisms in model diatoms. Current Opinion in Plant Biology. 31, 51-57.

Hopkinson BM, Meile C, Shen C. 2013. Quantification of Extracellular Carbonic Anhydrase Activity in Two Marine Diatoms and Investigation of Its Role. Plant Physiology. 162, 1142-1152.

Hu R, Yu H, Deng J, *et al.* 2025. Phosphoenolpyruvate and Related Metabolic Pathways Contribute to the Regulation of Plant Growth and Development. International Journal of Molecular Sciences. 26, 391.

Hughes CS, Foehr S, Garfield DA, Furlong EE, Steinmetz LM, Krijgsveld J. 2014. Ultrasensitive proteome analysis using paramagnetic bead technology. Molecular Systems Biology. 10, 757.

Inkscape Project. 2024. Inkscape v 1.4. https://inkscape.org

Intergovernmental Panel on Climate Change (IPCC). 2023. Climate Change 2021 – The Physical Science Basis: Working Group I Contribution to the Sixth Assessment Report of the Intergovernmental Panel on Climate Change. Cambridge: Cambridge University Press.

Jensen EL, Clement R, Kosta A, Maberly SC, Gontero B. 2019. A new widespread subclass of carbonic anhydrase in marine phytoplankton. The ISME Journal. 13, 2094–2106.

Kah LC, Riding R. 2007. Mesoproterozoic carbon dioxide levels inferred from calcified cyanobacteria. Geology. 35, 799-802.

Karlsson J, Ramazanov Z, Hiltonen T, Gardeström P, Samuelsson G. 1994. Effect of vanadate on photosynthesis and the ATP/ADP ratio in low-CO_2-adapted *Chlamydomonas reinhardtii* cells. Planta. 192, 46-51.

Kasting JF. 1993. Earth's early atmosphere. Science. 259, 920-926.

Kavanagh KL, Jörnvall H, Persson B, Oppermann U. 2008. The SDR superfamily: functional and structural diversity within a family of metabolic and regulatory enzymes. Cellular and Molecular Life Sciences. 65, 3895-3906.

Keller MD, Bellows WK, Guillard RRL. 1988. Microwave treatment for sterilization of phytoplankton culture media. Journal of Experimental Marine Biology and Ecology. 117, 279-283.

Kinoshita H, Nagasaki J, Yoshikawa N, Yamamoto A, Takito S, Kawasaki M, Sugiyama T, Miyake H, Weber APM, Taniguchi M. 2011. The chloroplastic 2-oxoglutarate/malate transporter has dual function as the malate valve and in carbon/nitrogen metabolism. The Plant Journal. 65, 15-26.

Kistner F, Grossmann JL, Sinn LR, Demichev V. 2023. QuantUMS: uncertainty minimization enables confident quantification in proteomics. bioRxiv. https://doi.org/10.1101/2023.06.20.545604. [Preprint].

Klusch N, Dreimann M, Senkler J, Rugen N, Kühlbrandt W, Braun HP. 2023. Cryo-EM structure of the respiratory I□+□III_2 supercomplex from Arabidopsis thaliana at 2□Å resolution. Nature Plants. 9, 142-156.

Koendjbiharie JG, van Kranenburg R, Kengen SWM. 2021. The PEP-pyruvate-oxaloacetate node: variation at the heart of metabolism. FEMS Microbiology Reviews. 45, 1-19.

Kuhn WR, Kasting JF. 1983. Effects of increased CO_2 concentrations on surface temperature of the early Earth. Nature. 53-55.

Kustka AB, Milligan AJ, Zheng H, New AM, Gates C, Bidle KD, Reinfelder JR. 2014. Low CO_2 results in a rearrangement of carbon metabolism to support C_4 photosynthetic carbon assimilation in *Thalassiosira pseudonana*. New Phytologist. 204, 607-520.

Laws EA, McClellan SA, Passow U. 2020. Interactive effects of CO_2 , temperature, irradiance, and nutrient limitation on the growth and physiology of the marine diatom *Thalassiosira pseudonana* (Coscinodiscophyceae). Journal of Phycology. 56, 1614-1624.

Lee K, Kim T-W, Byrne RH, Millero FJ, Feely RA, Liu Y-M. 2010. The universal ration of boron to chlorinity for the North Pacific and North Atlantic oceans. Geochimica et Cosmochimica Acta. 74, 1801–1811.

Leegood RC. 2002. C_4 photosynthesis: principles of CO_2 concentration and prospects for its introduction into C_3 plants. Journal of Experimental Botany. 53, 581-590.

Lewis ER, Wallace DWR. 1998. Program developed for CO_2 system calculations. (No. cdiac: CDIAC-105). Environmental System Science Data Infrastructure for a Virtual Ecosystem (ESS-DIVE), United States.

Liu S, Storti M, Finazzi G, Bowler C, Dorrell RG. 2022. A metabolic, phylogenomic and environmental atlas of diatom plastid transporters from the model species *Phaeodactylum*. Frontiers in Plant Science. 13, 950467.

Lourenço SO, Barbarino E, Lanfer Marquez UM, Aidar E. 1998. Distribution of intracellular nitrogen in marine microalgae: basis for the calculation of specific nitrogen-to-protein conversion factors. Journal of Phycology. 34, 798-811.

Lourenço SO, Barbarino E, Lavín PL, Lanfer Marquez UM, Aidar E. 2004. Distribution of intracellular nitrogen in marine microalgae: Calculation of new nitrogen-to-protein conversion factors. European Journal of Phycology. 39, 17–32.

Lu S, Wang J, Chitsaz F, *et al.* 2020. CDD/SPARCLE: the conserved domain database in 2020. Nucleic Acids Research. 48, D265-D268.

Lueker TJ, Dickson AG, Keeling CD. 2000. Ocean pCO_2 calculated from dissolved inorganic carbon, alkalinity, and equations for K_1 and K_2 : validation based on laboratory measurements of CO_2 in gas and seawater at equilibrium. Marine Chemistry. 70, 105–119.

Mackinder LCM, Meyer MT, Mettler-Altmann T, *et al.* 2016. A repeat protein links Rubisco to form the eukaryotic carbon-concentrating organelle. Proceedings of the National Academy of Sciences. 113, 21.

Maldonado M, Fan Z, Abe KM, Letts JA. 2023. Plant-specific features of respiratory supercomplex I□+□III_2 from *Vigna radiata*. Nature Plants. 9, 157-168.

Mamedov TG, Moellering ER, Chollet R. 2005. Identification and expression analysis of two inorganic C- and N-responsive genes encoding novel and distinct molecular forms of eukaryotic phosphoenolpyruvate carboxylase in the green microalga *Chlamydomonas reinhardtii*. The Plant Journal. 42, 832-843.

Marchler-Bauer A, Bo Y, Han L, *et al.* 2017. CDD/SPARCLE: functional classification of proteins via subfamily domain architectures. Nucleic Acids Research. 45, D200-D203.

Martínez-Reyes I, Chandel NS. 2020. Mitochondrial TCA cycle metabolites control physiology and disease. Nature Communications. 22, 102.

Mehrbach C, Culberson CH, Hawley JE, Pytkowicx RM. 1973. Measurement of the apparent dissociation constants of carbonic acid in seawater at atmospheric pressure. Limnology and Oceanography. 18, 897-907.

Meyer EH, Solheim C, Tanz SK, Bonnard G, Millar AH. 2011. Insights into the composition and assembly of the membrane arm of plant complex I through analysis of subcomplexes in Arabidopsis mutant lines. Journal of Biological Chemistry. 286, 26081-26092.

Mitra M, Mason CB, Xiao Y, Ynalvez RA, Lato SM, Moroney JV. 2005. The carbonic anhydrase gene families of *Chlamydomonas reinhardtii*. Canadian Journal of Botany. 83, 780-795.

Moellering ER, Ouyang Y, Mamedov TG, Chollet R. 2007. The two divergent PEP-carboxylase catalytic subunits in the green microalga Chlamydomonas reinhardtii respond reversibly to inorganic-N supply and co-exist in the high-molecular-mass, hetero-oligomeric Class-2 PEPC complex. FEBS Letters. 581, 4871-4876.

Moon HJ, Tiwari MK, Singh R, Kang YC, Lee JK. 2012. Molecular determinants of the cofactor specificity of ribitol dehydrogenase, a short-chain dehydrogenase/reductase. Applied and Environmental Microbiology. 78, 3079-3086.

Moroney JV, Ma Y, Frey WD, Fusilier KA, Pham TT, Simms TA, DiMario RJ, Yang J, Mukherjee B. 2011. The carbonic anhydrase isoforms of *Chlamydomonas reinhardtii*: intracellular location, expression, and physiological roles. Photosynthesis Research. 109, 133-149.

Mukherjee A, Lau CS, Walker CE, *et al.* 2019. Thylakoid localized bestrophin-like proteins are essential for the CO_2 concentrating mechanism of *Chlamydomonas reinhardtii*. Proceedings of the National Academy of Sciences USA. 116, 16915-16920.

Murik O, Tirichine L, Prihoda J, Thomas Y, Araújo WL, Allen AE, Fernie AR, Bowler C. 2018. Downregulation of mitochondrial alternative oxidase affects chloroplast function, redox status and stress response in a marine diatom. New Phytologist. 221, 1303-1316.

Nakajima K, Tanaka A, Matsuda Y. 2013. SLC4 family transporters in a marine diatom directly pump bicarbonate from seawater. Proceedings of the National Academy of Sciences USA. 110, 1767-72.

Nam O, Musiał S, Demulder M, McKenzie C, Dowle A, Dowson M, Barrett J, Blaza JN, Engel BD, Mackinder LCM. 2024. A protein blueprint of the diatom CO_2-fixing organelle. Cell. 187, 5935-5950.

Nawaly H, Matsui H, Tsuji Y, Iwayama K, Ohashi H, Nakajima K, Matsuda Y. 2023a. Multiple plasma membrane SLC4s contribute to external HCO_3^- acquisition during CO_2 starvation in the marine diatom *Phaeodactylum tricornutum*. Journal of Experimental Botany. 74, 296-307.

Nawaly H, Tanaka A, Toyoshima Y, Tsuji Y, Matsuda Y. 2023b. Localization and characterization θ carbonic anhydrases in *Thalassiosira pseudonana*. Photosynthesis Research. 156, 217-229.

Nawrocki WJ, Tourasse NJ, Taly A, Rappaport F, Wollman F-A. 2015. The plastid terminal oxidase: Its elusive function points to multiple contributions to plastid physiology. Annual Review of Plant Biology. 66, 49-74.

Nelson DM, Treguer P, Brzeezinski MA, Leynaert A, Queguiner B. 1995. Production and dissolution of biogenic silica in the ocean: Revised global estimates, comparison with regional data and relationship to biogenic sedimentation. Global Biogeochemical Cycle. 9, 359-372.

Nigishi M, Shimakawa G, Yamagishi K, Amano R, Ito S, Tsuji Y, Nagasato C, Matsuda Y. 2024. Low-CO_2-inducible bestrophins outside the pyrenoid sustain high photosynthetic efficacy in diatoms. Plant Physiology. 195, 1432-1445.

Novák Vanclová AMG, Dorrell RG. 2024. Complex Plastids Across the Eukaryotes: An overview of inherited and convergently evolved characters. In: Schwartzbach SD, Kroth PG, Oborník M (eds). Endosymbiotic Organelle Acquisition. Springer, Cham.

Occhipinti R, Boron WF. 2019. Role of carbonic anhydrases and inhibitors in acid-base physiology: Insights from mathematical modeling. International Journal of Molecular Sciences. 20, 3841.

Ødum MT, Teufel F, Thumuluri V, Almagro Armenteros JJ, Johansen AR, Winther O, Nielsen H. 2024. DeepLoc 2.1: multi-label membrane protein type prediction using protein language models. Nucleic Acids Research. 52, W215-W220.

O'Leary B, Plaxton WC. 2020. Multifaceted functions of post-translational enzyme modifications in the control of plant glycolysis. Current Opinion in Plant Biology. 55, 28-37.

O'Leary B, Park J, Plaxton WC. 2011. The remarkable diversity of plant PEPC (phosphoenolpyruvate carboxylase): recent insights into the physiological functions and post-translational controls of non-photosynthetic PEPCs. Biochemical Journal. 436, 15-34.

O'Leary B, Rao SK, Kim J, Plaxton WC. 2009. Bacterial-type phosphoenolpyruvate carboxylase (PEPC) functions as a catalytic and regulatory subunit of the novel class-2 PEPC complex of vascular plants. The Journal of Biological Chemistry. 284, 24797-24805.

Park J, Khuu N, Howard AS, Mullen RT, Plaxton WC. 2012. Bacterial- and plant-type phosphoenolpyruvate carboxylase isozymes from developing castor oil seeds interact in vivo and associate with the surface of mitochondria. The Plant Journal. 71, 251-262.

Parker MS, Armbrust EV. 2005. Synergistic effects of light, temperature, and nitrogen source on transcription of genes for carbon and nitrogen metabolism in the centric diatom *Thalassiosira pseudonana*. Journal of Phycology. 41, 1142-1153.

Parisi G, Perales M, Fornasari MS, *et al.* 2004. Gamma carbonic anhydrases in plant mitochondria. Plant Molecular Biology. 55, 193-207.

Perales M, Eubel H, Heinemeyer J, Colaneri A, Zabaleta E, Braun HP. 2005. Disruption of a nuclear gene encoding a mitochondrial gamma carbonic anhydrase reduces complex I and supercomplex I + III_2 levels and alters mitochondrial physiology in *Arabidopsis*. Journal of Molecular Biology. 350, 263-277.

Perez FF, Fraga F. 1987. Association constant of fluoride and hydrogen ions in seawater. Marine Chemistry. 21, 161–168.

Perez-Riverol Y, Bandla C, Kundu DJ, *et al*. 2025. The PRIDE database at 20 years: 2025 update. Nucleic Acids Res. 53, D543-D553.

Persily A, Gorfain J. 2009. Analysis of ventilation data from the U.S. Environmental Protection Agency building assessment survey and evaluation (BASE) study. National Institute of Standards and Technology interagency/internal report 7145-R.

Poschenrieder C, Fernández JA, Rubio L, Pérez L, Terés J, Barceló J. 2018. Transport and use of bicarbonate in plants: Current knowledge and challenges ahead. International Journal of Molecular Sciences. 19, 1352.

Qu Z, Hartzell HC. 2008. Bestrophin Cl^- channels are highly permeable to HCO_3^-. American Journal of Physiology-Cell Physiology. 294, C1371-C1377.

R Core Team 2024. R: A Language and Environment for Statistical Computing. R Foundation for Statistical Computing, Vienna, Austria. https://www.R-project.org.

Raven JA. 2001. A role for mitochondrial carbonic anhydrase in limiting CO_2 leakage from low CO_2-grown cells of *Chlamydomonas reinhardtii*. Plant, Cell and Environment. 24, 261-265.

Reinfelder JR. 2011. Carbon concentrating mechanisms in eukaryotic marine phytoplankton. Annual Review of Marine Science. 3, 291-315.

Reinfelder JR, Milligan AJ, Morel FMM. 2004. The role of the C_4 pathway in carbon accumulation and fixation in a marine diatom. Plant Physiology. 135, 2106-2111.

Rivoal J, Dunford R, Plaxton WC, Turpin DH. 1996. Purification and properties of four phosphoenolpyruvate carboxylase isoforms from the green alga *Selenastrum minutum*: evidence that association of the 102-kDa catalytic subunit with unrelated polypeptides may modify the physical and kinetic properties of the enzyme. Archives of Biochemistry and Biophysics. 332, 47-57.

Rivoal J, Plaxton WC, Turpin DH. 1998. Purification and characterization of high- and low-molecular-mass isoforms of phosphoenolpyruvate carboxylase from *Chlamydomonas reinhardtii*. Kinetic, structural and immunological evidence that the green algal enzyme is distinct from the prokaryotic and higher plant enzymes. Biochemistry Journal. 331, 201-209.

Rivoal J, Turpin DH, Plaxton WC. 2002. In vitro phosphorylation of phosphoenolpyruvate carboxylase from the green alga *Selenastrum minutum*. Plant & Cell Physiology. 43, 785-792.

Roberts K, Granum E, Leegood RC, Raven JA. 2007. C_3 and C_4 pathways of photosynthetic carbon assimilation in marine diatoms are under genetic, not environmental, control. Plant Physiology. 145, 230-235.

Rousseaux CS, Gregg WW. 2014. Interannual variation in phytoplankton primary production at a global scale. Remote Sensing. 6, 1-19.

Sakano K. 1998. Revision of biochemical pH-stat: Involvement of alternative pathway metabolisms. Plant Cell Physiology. 39, 467-473.

Samukawa M, Shen C, Hopkinson BM, Matsuda Y. 2014. Localization of putative carbonic anhydrases in the marine diatom, *Thalassiosira pseudonana*. Photosynthesis Research. 121, 235-249.

Schober AF, Rï O Bï Rtulos C, Bischoff A, Lepetit B, Gruber A, Kroth PG. 2019. Organelle studies and proteome analyses of mitochondria and plastids fractions from the diatom *Thalassiosira pseudonana*. Plant Cell Physiol. Plant Cell Physiology. 60, 1811-1828.

Schüter U, Weber APM. 2020. Regulation and evolution of C_4 photosynthesis. Annual Review of Plant Biology. 71, 183-215.

Selinski J, Scheibe R. 2018. Malate valves: old shuttles with new perspectives. Plant Biology. 21, 21-30.

Shikanai T. 2007. Cyclic electron transport around photosystem I: Genetic approaches. Annual Review of Plant Biology. 58, 199-217.

Shimakawa G, Demulder M, Flori S, *et al.* 2024. Diatom pyrenoids are encased in a protein shell that enables efficient CO_2 fixation. Cell. 187, 5919-5934.

Shimakawa G, Yashiro E, Matsuda Y. 2023. Mapping of subcellular local pH in the marine diatom *Phaeodactylum tricornutum*. Physiologia Plantarum. 175, e14086.

Shi D, Li W, Hopkinson BM, Hong H, Li D, Kao S-J, Lin W. 2015. Interactive effects of light, nitrogen source, and carbon dioxide on energy metabolism in the diatom *Thalassiosira pseudonana*. Limnology and Oceanography. 60, 1805-1822.

Shi D, Xu Y, Morel FMM. 2009. Effects of the pH/pCO_2 control method on medium chemistry and phytoplankton growth. Biogeosciences. 6, 119-1207.

Shi Q, Xiahou W, Wu H. 2017. Photosynthetic responses of the marine diatom *Thalassiosira pseudonana* to CO_2-induced seawater acidification. Hydrobiologia. 788, 361-369.

Soto D, Córdoba JP, Villarreal F, Bartoli C, Schmitz J, Maurino VG, Braun HP, Pagnussat GC, Zabaleta E. 2015. Functional characterization of mutants affected in the carbonic anhydrase domain of the respiratory complex I in *Arabidopsis thaliana*. The Plant Journal. 83, 831-844.

Stramski D, Sciandra A, Claustre H. 2002. Effects of temperature, nitrogen, and light limitation on the optical properties of the marine diatom *Thalassiosira pseudonana*. Limnology and Oceanography. 47, 392-403.

Sticker A, Goeminne L, Martens L, Clement L. 2020. Robust Summarization and Inference in Proteome-wide Label-free Quantification. Molecular & Cellular Proteomics. 19, 1209-1219.

Sunda WG, Price NM, Morel FMM. 2005. Trace metal ion buffers and their use in culture studies. In: Andersen RA (Ed.), Algal culturing techniques, Elsevier Academy Press, 35–63.

Sunderhaus S, Dudkina NV, Jänsch L, Klodmann J, Heinemeyer J, Perales M, Zabaleta E, Boekema EJ, Braun HP. 2006. Carbonic anhydrase subunits form a matrix-exposed domain attached to the membrane arm of mitochondrial complex I in plants. Journal of Biological Chemistry. 281, 6482-6488.

Supuran CT. 2016. Structure and function of carbonic anhydrases. Biochemical Journal. 473, 2023-2032.

Tachibana M, Allen AE, Kikutani S, Endo Y, Bowler C, Matsuda Y. 2011. Localization of putative carbonic anhydrases in two marine diatoms, *Phaeodactylum tricornutum* and *Thalassiosira pseudonana*. Photosynthesis Research. 109, 205-221.

Tanaka R, Kikutani S, Mahardika A, Matsuda Y. 2014. Localization of enzymes relating to C_4 organic acid metabolisms in the marine diatom, *Thalassiosira pseudonana*. Photosynthesis research. 121, 251-263.

Taniguchi M, Taniguchi Y, Kawasaki M, Takeda S, Kato T, Sato S, Tabata S, Miyake H, Sugiyama T. 2002. Identifying and characterizing plastidic 2-oxoglutarate/malate and dicarboxylate transporters in *Arabidopsis thalia*na. Plant Cell Physiology. 43, 706-717.

Thielmann J, Tolbert NE, Goyal A, Senger H. 1990 Two systems for concentrating CO_2 and bicarbonate during photosynthesis by *Scenedesmus*. Plant Physiology. 92, 622-629.

Thompson P. 1999. The response of growth and biochemical composition to variations in daylength, temperature, and irradiance in the marine diatom *Thalassiosira pseudonana* (Bacillariophyceae). Journal of Phycology. 35, 1215-1223.

Thompson PA, Harrison PJ, Whyte JNC. 1990. Influence of irradiance on the fatty acid composition of phytoplankton. Journal of Phycology. 26, 278-288.

Ting MKY, She YM, Plaxton WC. 2017. Transcript profiling indicates a widespread role for bacterial-type phosphoenolpyruvate carboxylase in malate-accumulating sink tissues. Journal of Experimental Botany. 68, 5857-5869.

Tréguer P, Bowler C, Moriceau B, *et al.* 2018. Influence of diatom diversity on the ocean biological carbon pump. Nature Geoscience. 11, 27-37.

Trimborn S, Lundholm N, Thoms S, Richter K-U, Krock B, Hansen PJ, Rost B. 2008. Inorganic carbon acquisition in potentially toxic and non-toxic diatoms: the effect of pH-induced changes in seawater carbonate chemistry. Physiologia Plantarum. 133, 92-105.

Trimborn S, Wolf-Gladrow D, Richter K-U, Rost B. 2009 The effect of pCO_2 on carbon acquisition and intracellular assimilation in four marine diatoms. Journal of Experimental Marine Biology and Ecology. 376, 26-36.

Tronconi MA, Andreo CS, Drincovich MF. 2018. Chimeric Structure of Plant Malic Enzyme Family: Different Evolutionary Scenarios for NAD- and NADP-Dependent Isoforms. Frontiers in Plant Science. 9, 565.

Tsuji Y, Mahardika A, Matsuda Y. 2017. Evolutionarily distinct strategies for the acquisition of inorganic carbon from seawater in marine diatoms. Journal of Experimental Botany. 68, 3949-3958.

Tsuji Y, Kusi-Appiah G, Kozai N, Fukuda Y, Yamano T, Fukuzawa H. 2021. Characterization of a CO_2-concentrating mechanism with low sodium dependency in the centric diatom *Chaetoceros gracilis*. Marine Biotechnology. 23, 456-462.

van Dongen JT, Gupta KJ, Ramírez-Aguilar SJ, Araújo WL, Nunes-Nesi A, Fernie AR. 2011. Regulation of respiration in plants: A role for alternative metabolic pathways. Journal of Plant Physiology. 168, 1434-1443.

Vanlerberghe GC, Dahal K, Alber NA, Chadee A. 2020. Photosynthesis, respiration and growth: A carbon and energy balancing act for alternative oxidase. Mitochondrion. 52, 197-211.

Wang J, Chitsaz F, Derbyshire MK, *et al.* 2023. The conserved domain database in 2023. Nucleic Acids Research. 51, D384-D388.

Wang Y, Stessman DJ, Spalding MH. 2015. The CO_2 concentrating mechanism and photosynthetic carbon assimilation in limiting CO_2: how Chlamydomonas works against the gradient. The Plant Journal. 82, 429-448.

Westberry TK, Silsbe GM, Behrenfeld MJ. 2023. Gross and net primary production in the global ocean: An ocean color remote sensing perspective. Earth-Science Reviews. 237, 104322.

Wickham H. 2016. ggplot2: Elegant Graphics for Data Analysis. Springer-Verlag New York.

Wu S, Gu W, Jia S, Wang L, Wang L, Liu X, Zhou L, Huang A, Wang G. 2021. Proteomic and biochemical responses to different concentrations of CO_2 suggest the existence of multiple carbon metabolism strategies in *Phaeodactylum tricornutum.* Biotechnology for Biofuels. 12, 235.

Yamori W, Shikanai T, Makino A. 2015. Corrigendum: Photosystem I cyclic electron flow via chloroplast NADH dehydrogenase-like complex performs a physiological role for photosynthesis at low light. Scientific Reports. 5, 15593.

Yoshida K, Terashima I, Noguchi K. 2007. Up-regulation of mitochondrial alternative oxidase concomitant with chloroplast over-reduction by excess light. Plant Cell Physiology. 48, 606-614.

Yu Q, Feilke K, Krieger-Liszkay A, Beyer P. 2014. Functional and molecular characterization of plastid terminal oxidase from rice (*Oryza sativa*). Biochimica et Biophysica Acta. 1837, 1284-1292.

Yu G, Nakajima K, Gruber A, Rio Bartulos C, Schober AF, Lepetit B, Yohannes E, Matsuda Y, Kroth PG. 2022. Mitochondrial phosphoenolpyruvate carboxylase contributes to carbon fixation in the diatom *Phaeodactylum tricornutum* at low inorganic carbon concentrations. New Phytologist. 235, 1379-1393.

Zabaleta E, Martin MV, Braun H-P. 2012. A basal carbon concentrating mechanism in plants? Plant Science. 187, 97-104.

Zara V, Assalve G, Ferramosca A. 2022. Multiple roles played by the mitochondrial citrate carrier in cellular metabolism and physiology. Cellular and Molecular Life Sciences. 79, 428.

Zhang Y, Yin L, Jiang H-S, Li W, Gontero B, Maberly SC. 2014. Biochemical and biophysical CO 2 concentrating mechanisms in two species of freshwater macrophyte within the genus *Ottelia* (Hydrocharitaceae). Photosynthesis Research. 121, 285-297.

Zhen Y, Zhu J, Yue M, Mi T. 2025. Impacts of phosphoenolpyruvate carboxylase gene silencing on photosynthetic efficiency and carbon fixation in *Skeletonema costatum*. Gene. 933, 148915.

Zhou L, Wu S, Gu W, Wang L, Wang J, Gao S, Wang G. 2021. Photosynthesis acclimation under severely fluctuating light conditions allows faster growth of diatoms compared with dinoflagellates. BMC Plant Biology. 21, 164.

Tables and Figures

Table 1 Experimental culture conditions.

Treatment	Temperature set point (°C)	Target pCO_2 (µatm)	pH_{NBS}	Growth rate (d^{-1})
LCHpH	18	202	8.45 ± 0.02	1.98 ± 0.07
HCLpH	18	1702	7.60 ± 0.01	2.00 ± 0.08
LCLpH	18	202	7.58 ± 0.03	2.03 ± 0.08

pH_{NBS} and growth rates reported as mean ± SD. For all treatment levels n = 8.

Table 2 Differential abundance of key proteins with hypothesized roles in a CCM, pH homeostasis mechanism, cyclic electron transport pathway, and/or excess energy dissipation pathway.

Uniprot ID	Description	Name	Average fold change LCHpH v HCLpH	Average fold change LCHpH v LCLpH	Source
B8C0D8	Bestrophin 1	TpBST1	2.09	-	Nigishi et al., 2024
B8C0D9	Bestrophin 2	TpBST2	2.81	-	Nigishi et al., 2024
B8C0V5	α carbonic anhydrase 3	TpαCA3	-1.35	-	Samukawa et al., 2014
W8VYH0	δ carbonic anhydrase 1	TpδCA1	5.10	-	Samukawa et al., 2014
W8VSK0	γ carbonic anhydrase 1	TpγCA1	-	-	Samukawa et al., 2014
B8C215	γ carbonic anhydrase 4	TpγCA4	-	-	Samukawa et al., 2014
W8VLR1	γ carbonic anhydrase like protein	TpγCAL	-	-	Samukawa et al., 2014; Cainzos et al., 2021
B8LE19	θ carbonic anhydrase 1	TpθCA1	2.39	-	Nawaly et al., 2023
B8BPY6	θ carbonic anhydrase 2	TpθCA2	1.40	-	Nawaly et al., 2023
B8LE17	θ carbonic anhydrase 3	TpθCA3	1.75	-	Nawaly et al., 2023
B8C3H8	θ carbonic anhydrase 4	TpθCA4	-3.57	-	Nawaly et al., 2023
B8CG97	ζ carbonic anhydrase 1	TpζCA1	9.69	-	Tachibana et al., 2011
B8LE18	LCIP carbonic anhydrase domain-containing protein		5.98	-	Armbrust et al., 2004; Bowler et al., 2008
B5YNR1	Malate dehydrogenase	MDH_c	1.55	-	Armbrust et al., 2004; Bowler et al., 2008
B8CF37	Mitochondrial alternative oxidase 1	AOX1	-	-	Armbrust et al., 2004; Bowler et al., 2008
B8CF38	Mitochondrial alternative oxidase 2	AOX2	-	-	Armbrust et al., 2004; Bowler et al., 2008
B8LBH6	NADH:ubiquinone reductase (non-electrogenic)		-	-	Armbrust et al., 2004; Bowler et al., 2008
W8VUB7	NAD-dependent malic enzyme	NAD-ME	-	-	Tanaka et al., 2014
B8LBP8	NAD(P)-binding domain-containing protein		1.33	-	Armbrust et al., 2004; Bowler et al., 2008
B8C9Q9	Oxoglutarate/malate translocator	OMT	-	-	Armbrust et al., 2004; Bowler et al., 2008
W8VKT0	Phosphoenolpyruvate carboxylase 1	PEPC1	-	-	Tanaka et al., 2014

W8VLS4	Phosphoenolpyruvate carboxylase 2	PEPC2	1.32	-	Tanaka et al., 2014
W8VYH5	Phosphoenolpyruvate carboxykinase	PEPCK	-2.78	-	Tanaka et al., 2014
B8CC74	Plastidial terminal oxidase 1	PTOX1	ND	ND	Nawrocki et al., 2015
B8LD44	Plastidial terminal oxidase 2	PTOX2	-	-	Nawrocki et al., 2015
B8C035	Proton gradient regulation 5 protein	PGR5	-	-	Zhou et al., 2021
B8BZQ3	PGR5-like photosynthetic phenotype 1 protein	PGRL1	-	-	Hertle et al., 2013

Uniprot ID numbers provided, but descriptions have been updated with more recent information as cited. Differential abundance (> 1.3 fold-change and adjusted $P < 0.05$; Benjamini-Hochberg method) is shown as the average fold change in the LCHpH treatment compared to either the HCLpH or LCLpH treatments (n = 4 for all treatments). Positive fold changes indicate greater protein abundance in LCHpH grown cells while negative values denote lower abundance in LCHpH grown cells. Dashes indicate that no significant difference in abundance was detected. ND indicates the protein was not sufficiently detected for accurate quantification.

Table 3 Steady state culture conditions, growth rates, and final culture sampling densities reported from a selection of *T. pseudonana* CCM studies cited within the present work.

Study	Treatment name	pH	(p)CO_2	$NaHCO_3$ (mM)	Light intensity (µmol photon m^{-2} s^{-1})	Light:dark cycle (h)	Temperature (°C)	Growth rate	Final sampling density
Granum et al., 2005	Ambient	NR	400 ppm	2.38*	200	12:12	15	1 d^{-1}	NR
	Low	NR	100 ppm	2.38*	200	12:12	15	1 d^{-1}	NR
Roberts et al., 2007	Near ambient	8.1	380 µL L^{-1}	2.4	200	12:12	15	≥ 1 d^{-1}	NR
	Low	NR	100 µL L^{-1}	0.6	200	12:12	15	≥ 1 d^{-1}	NR
Granum et al., 2009	Near ambient	NR	380 µL L^{-1}	2.4	200	12:12	15	1.4 d^{-1}	NR
	Low	NR	100 µL L^{-1}	0.6	200	12:12	15	1.4 d^{-1}	NR
Trimborn et al., 2009	High pCO_2	7.90 ± 0.03	800 µatm	NR	200	16:8	15	NR	NR
	Ambient pCO_2	8.20 ± 0.03	370 µatm	NR	200	16:8	15	NR	NR
	Low pCO_2	8.85 ± 0.03	50 µatm	NR	200	16:8	15	NR	NR
Tachibana et al., 2011	High CO_2	NR	1600 ppm	2.066*	50	24:0	20	NR	OD_{730} = 0.2
	Air	NR	NR	2.066*	50	24:0	20	NR	OD_{730} = 0.2
Hopkinson et al., 2013	Control	8.4	NR	NR	125-150	16:8	20	1.15 ± 0.01 d^{-1}	NR

Kustka et al., 2014	High CO_2	7.61	1780 µL L^{-1}	2.38	200	24:0	18	2.06 ± 0.01 d^{-1}	(4–5) x 10^5 cells mL^{-1}
	Low CO_2	8.48	210 µL L^{-1}	2.38	200	24:0	18	2.03 ± 0.07 d^{-1}	(4–5) x 10^5 cells mL^{-1}
Samukawa et al., 2014	High CO_2	NR	4000 ppm	2.066*	50	24:0	20	NR	OD_{730} = 0.15
	Air	NR	400 ppm	2.066*	50	24:0	20	NR	OD_{730} = 0.15
Tanaka et al., 2014	High CO_2	NR	2000 ppm	2.066*	50	24:0	20	NR	OD_{730} = 0.2
	Air	NR	NR	2.066*	50	24:0	20	NR	OD_{730} = 0.2
Clement et al., 2016	Extremely high	6.9	20,000 ppm	1.71	50	24:0	16	0.70 ± 0.01 d^{-1}	NR
	Air	7.9†	400 ppm	1.71	50	24:0	16	0.54 ± 0.02 d^{-1}	NR
Clement et al., 2017	High CO_2	NR	20,000 ppm	1.71*	50	24:0	16	NR	NR
	Air	NR	400 ppm	1.71*	50	24:0	16	NR	NR
Shi et al., 2017	Projected 2100	7.89 ± 0.04	800 µatm	2.38	180	14:10	20	1.10 ± 0.03 d^{-1}	< 3 x 10^5 cells mL^{-1}
	Outdoor ambient	8.24 ± 0.03	380 µatm	2.38	180	14:10	20	1.23 ± 0.02 d^{-1}	< 3 x 10^5 cells mL^{-1}
Nawaly et al., 2023b	High CO_2	NR	10,000 ppm	2.066*	50	24:0	20	1.80 divisions d^{-1}‡	OD_{730} = 0.1–0.15
	Low CO_2	NR	400 ppm	2.066*	50	24:0	20	1.65 divisions d^{-1}‡	OD_{730} = 0.1–0.15
Nigishi et al., 2024	High CO_2	NR	10,000 ppm	2.066*	40	24:0	20	NR	NR
	Low CO_2	NR	400 ppm	2.066*	40	24:0	20	NR	NR
This study	LCHpH	8.45 ± 0.02	202 µatm	2.38	250	24:0	18	1.98 ± 0.07 d^{-1}	7 x 10^4 cells mL^{-1}
	HCLpH	7.60 ± 0.01	1702 µatm	2.38	250	24:0	18	2.00 ± 0.08 d^{-1}	7 x 10^4 cells mL^{-1}
	LCLpH	7.58 ± 0.03	202 µatm	0.283	250	24:0	18	2.03 ± 0.08 d^{-1}	7 x 10^4 cells mL^{-1}

NR, not reported. *Value taken from the literature cited for the media recipe used. †pH started at 7.9 but increased to ~9.2, pH stayed above 9 for the remaining four days of the growth experiment. ‡Estimated from Fig. 5 in Nawaly *et al.*, 2023b.

Fig. 1. Venn diagrams depicting the number of proteins that were more abundant (left) or less abundant (right) in the LCHpH treatment compared to either the HCLpH (green) or LCLpH (purple) treatments. Overlap indicates differentially expressed proteins shared between both low pH conditions. Graphic generated in Inkscape (Inkscape Project, 2024).

ALT TEXT: Venn diagrams of the total number of proteins that were either more or less abundant in each of the two treatment comparisons.

Fig. 2. Volcano plots showing changes in protein expression for A) LCHpH compared to HCLpH and B) LCHpH compared to LCLpH. Data shown as $-\log_{10}$ of the adjusted P value plotted against $\log_2$ of the protein abundance fold change. The dashed horizontal line indicates $\alpha = 0.05$. The dashed vertical lines indicate the *a priori* 1.30 protein fold-change significance threshold. Red triangles represent proteins with significantly different abundances between treatment groups while gray circles represent proteins that did not cross both significance thresholds. The data point markers are shown to the right of the labels, which correspond to Uniprot IDs listed in Table 2. Overlapping labels were removed for readability. Plots produced with ggplot2 R package ver. 3.5.1 (Wickham, 2016).

ALT TEXT: Graphs showing the statistical results for all 7,803 proteins that passed quality control filtering in each of the two treatment comparisons evaluated in this study.

Fig. 3. Cross section of a *T. pseudonana* cell showing the schematic of the proposed CCM. Concentric circles starting from the outside moving in represent the frustule, plasma membrane, and the four membranes of the complex plastid. Each step of the CCM is numbered following the subheadings within the discussion. **Step 1:** the conversion of extracellular HCO_3^- to CO_2 by TpδCA1 and TpζCA1 which then diffuses across the plasma membrane. **Step 2:** the conversion of this influxing CO_2 back to HCO_3^- potentially by TpαCA3 and TpθCA4. **Step 3:** the carboxylation of PEP and HCO_3^- to OAA by PEPC2 (or the class 2 PEPC complex). **Step 4:** the conversion of this OAA to malate by MDH_c. **Step 5:** the translocation of malate into the chloroplast by an as yet unknown carboxylate transporter before the unknown stromal decarboxylase releases CO_2 from malate. **Step 6:** the conversion of CO_2 produced by the decarboxylase into HCO_3^- by TpθCA1 and TpθCA3 before HCO_3^- then diffuses down its concentration gradient through bestrophin 1 and 2 into the PPT. **Step 7:** TpθCA2 within the PPT lumen converts influxing HCO_3^- back to CO_2, which then passively diffuses out to RuBisCO in the pyrenoid. The black box titled recapture across the mitochondrial membranes corresponds to the zoomed in view of the proposed CO_2 recapture mechanism shown in Figure 4. Cellular components are not shown to scale. Abbreviations ordered stepwise: δ1, delta-type carbonic anhydrase 1; ζ1, zeta-type carbonic anhydrase 1; α3, alpha-type carbonic anhydrase 3; θ4, theta-type carbonic anhydrase 4; PEP, phosphoenolpyruvate; PEPC2, phosphoenolpyruvate carboxylase 2; OAA, oxaloacetate; MDH_c, cytoplasmic form of malate dehydrogenase; CT?, unknown carboxylate transporter; DE?, unknown decarboxylase; θ1, theta-type carbonic anhydrase 1; θ3, theta-type carbonic anhydrase 3; B1, bestrophin 1; B2, bestrophin 2; PPT, pyrenoid-penetrating thylakoid; θ2, theta-type carbonic anhydrase 2. Graphic generated in Inkscape (Inkscape Project, 2024).

ALT TEXT: A visual schematic of the proposed carbon concentrating mechanism within a *T. pseudonana* cell informed by statistically significant differential protein abundance data generated in this study.

Fig. 4. Magnified view of a portion of a mitochondrion within *T. pseudonana* showing the proposed CO_2 recapture mechanism. CO_2 is produced as a byproduct of the tricarboxylic acid (TCA) cycle in the mitochondrial matrix and begins to diffuse out of the mitochondrion. Once CO_2 reaches the inner mitochondrial membrane it encounters the γCA domain, which is composed of three heterogeneous subunits, within a portion of complex I that extends into the matrix. The γCA domain converts CO_2 to HCO_3^- which leaves the mitochondrion through unknown HCO_3^- channels out to PEPC2 (or the class 2 PEPC complex). PEPC2 then converts this HCO_3^- and PEP into OAA, which continues on into step 4 of the CCM shown in Figure 3. Cellular components are not shown to scale. Abbreviations: C1, mitochondrial electron transport chain complex 1; γ1, gamma-type carbonic anhydrase 1; γ4, gamma-type carbonic anhydrase 4; γL, gamma-type carbonic anhydrase like protein; HCO_3^- Ch?, unknown bicarbonate channel; PEP, phosphoenolpyruvate; PEPC2, phosphoenolpyruvate carboxylase 2; OAA, oxaloacetate. Graphic generated in Inkscape (Inkscape Project, 2024).

ALT TEXT: A zoomed in view of the proposed CO_2 recapture mechanism indicated by the black box insert in Fig. 3. Schematic shows the process through which CO_2 released in the mitochondrial matrix can be recaptured and fed back into the CCM.

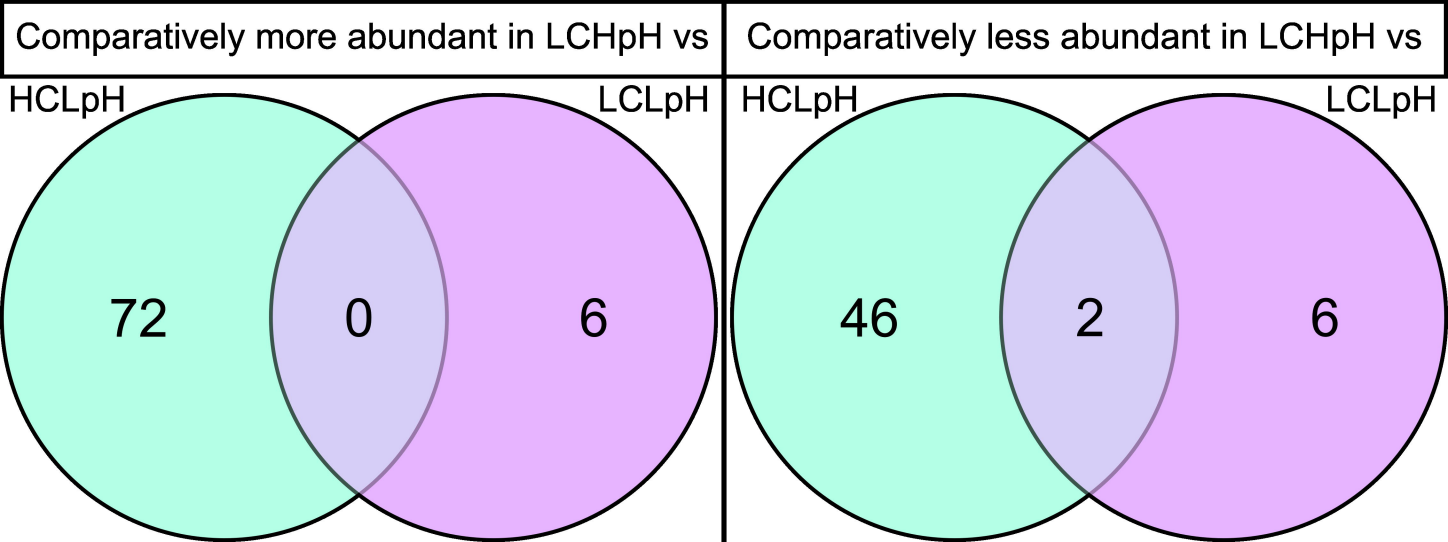
Comparatively more abundant in LCHpH vs
HCLpH
LCLpH
72
0
6
Comparatively less abundant in LCHpH vs
HCLpH
LCLpH
46
2
6

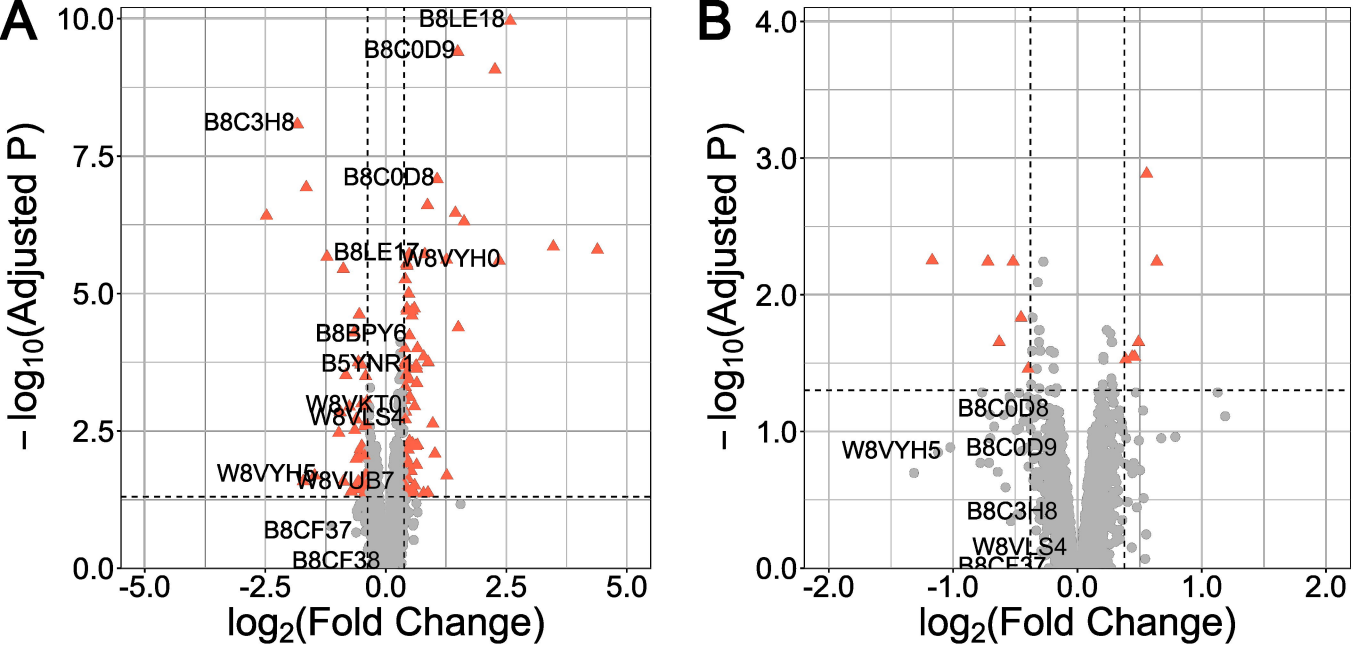
A
B
B8LE18
B8C0D9
B8C3H8
B8C0D8
B8LE17
W8VYH0
B8BPY6
B5YNR1
W8VKT0
W8VLS4
W8VYH5
W8VUB7
B8CF37
B8CF38
B8C0D8
W8VYH5
B8C0D9
B8C3H8
W8VLS4
B8CF37
10.0
7.5
5.0
2.5
0.0
4.0
3.0
2.0
1.0
0.0
-5.0
-2.5
0.0
2.5
5.0
-2.0
-1.0
0.0
1.0
2.0
$-\log_{10}$(Adjusted P)
$\log_2$(Fold Change)

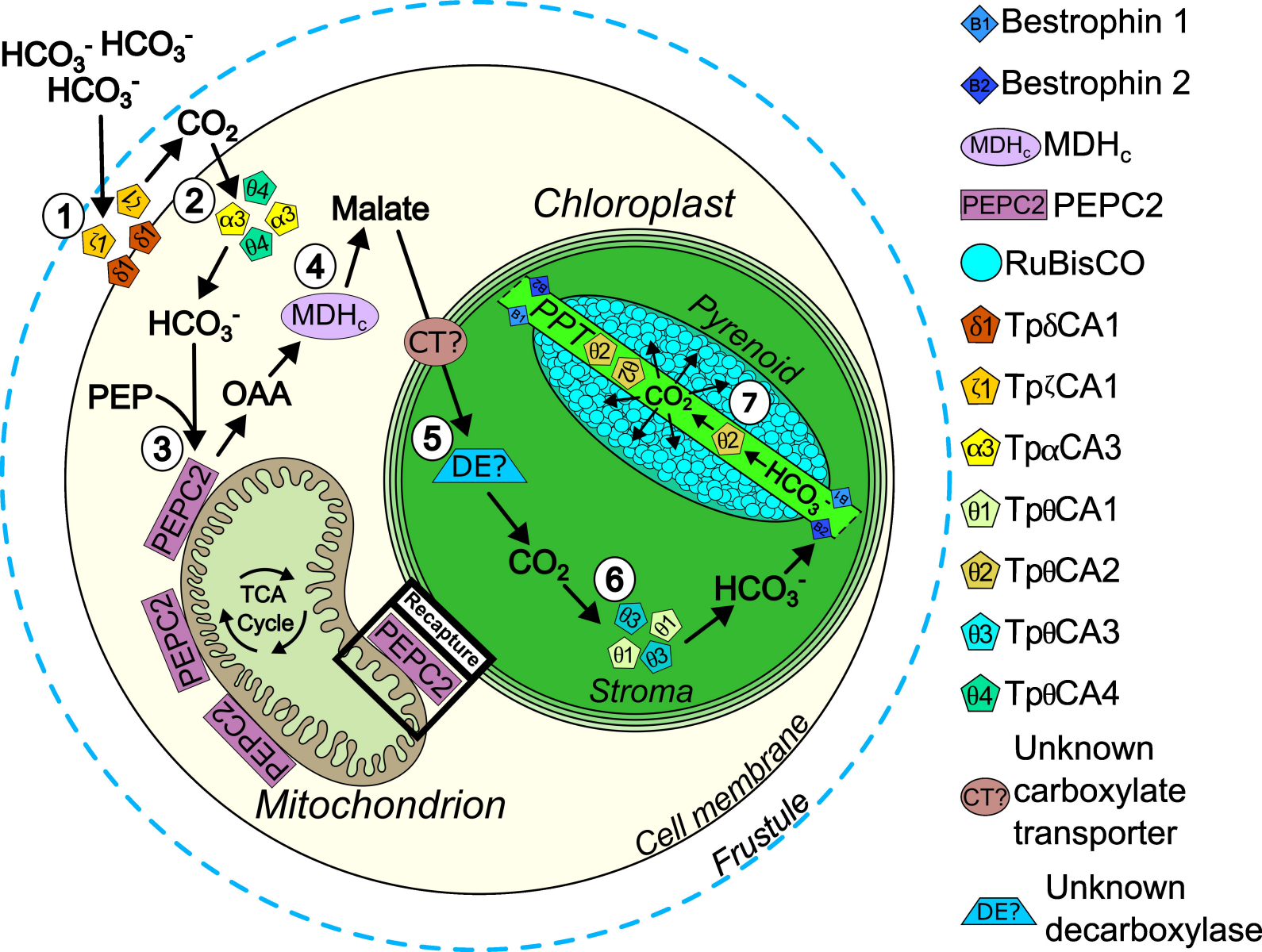

HCO3- HCO3-
HCO3-
CO2
1
2
3
4
5
6
7
ζ2
ζ1
δ1
δ1
θ4
α3
α3
θ4
HCO3-
PEP
OAA
MDHc
Malate
CT?
DE?
Chloroplast
Pyrenoid
PPT
θ2
θ2
CO2
θ2
HCO3-
CO2
HCO3-
θ3
θ1
θ1
θ3
Stroma
PEPC2
PEPC2
PEPC2
PEPC2
TCA Cycle
Recapture
Mitochondrion
Cell membrane
Frustule
B1 Bestrophin 1
B2 Bestrophin 2
MDHc MDHc
PEPC2 PEPC2
RuBisCO
δ1 TpδCA1
ζ1 TpζCA1
α3 TpαCA3
θ1 TpθCA1
θ2 TpθCA2
θ3 TpθCA3
θ4 TpθCA4
CT? Unknown carboxylate transporter
DE? Unknown decarboxylase

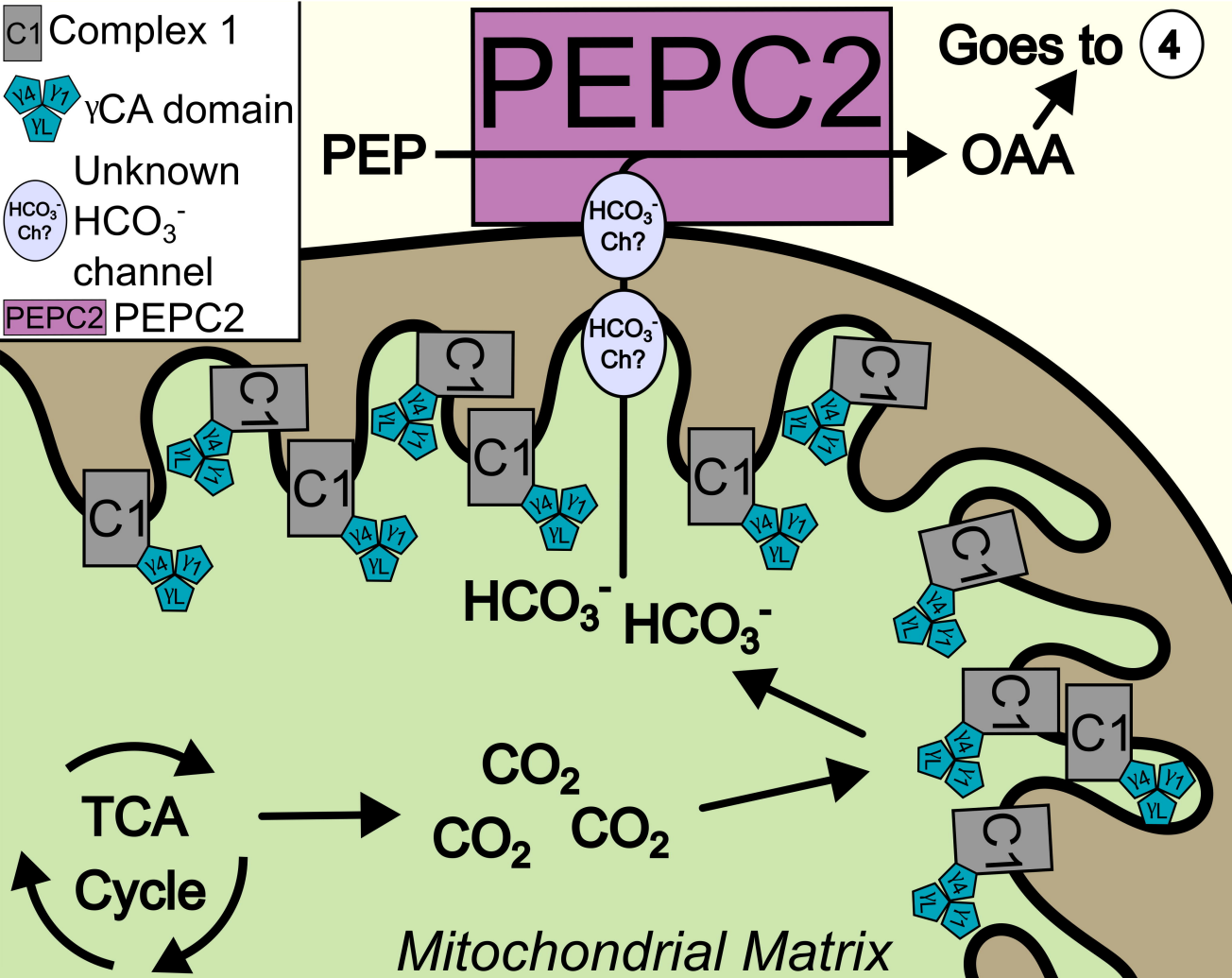
C1 Complex 1
γCA domain
Unknown HCO3- channel
PEPC2 PEPC2
PEPC2
PEP
OAA
Goes to 4
HCO3- Ch?
HCO3- Ch?
C1
HCO3-
HCO3-
TCA Cycle
CO2
CO2
CO2
Mitochondrial Matrix